Meso-β-scale Pressure Dips Associated with Typhoons

Hironori Fudeyasu* and Satoshi Iizuka

National Research Institute for Earth Science and Disaster Prevention, Tsukuba, Japan

Taiichi Hayashi

Disaster Prevention Research Institute, Kyoto University, Kyoto, Japan

ABSTRACT

Using a mesoscale model, the formation process of a pressure dip, which was characterized by a rapid decrease and subsequent increase in surface pressure lasting less than an hour, was investigated. A simulated pressure dip accompanied by Typhoon Zeb was closely related to warm potential temperature anomalies in the lower troposphere. As the typhoon moved into the midlatitude westerlies, the inflow of a dry air mass into the moist region of the typhoon occurred to the west of the typhoon center. Then, a downdraft developed due to evaporation and sublimation. Below the melting levels where there were fewer hydrometeors, however, evaporation was insufficient to offset the adiabatic warming. As a result, warm potential temperature anomalies were created in the lower level, resulting in the formation of a pressure dip. The features of a pressure dip associated with other typhoons observed over Japan were also examined. The features were summarized as follows: 1) the pressure dip was observed only on the western side of the typhoon center at a distance of 50–300 km from the center, 2) the pressure dip was accompanied by a sudden cessation of rainfall, and 3) all typhoons with a pressure dip were found during boreal autumn when large-scale environmental conditions were characterized by westerlies with a trough and a dry air mass to the west of Japan at upper levels and fronts at lower levels. The formation process of the simulated pressure dip in other typhoons was found to be similar to that of Typhoon Zeb. The present study suggests that pressure dip is an inherent feature of the asymmetric structure of a typhoon undergoing transition to a extratropical cyclone.

1. Introduction

Fujita (1952) first described the phenomenon of a pressure dip that is occasionally observed in association with typhoons crossing the Japanese islands or moving along the southern coast of Japan (e.g., Nakajima et al. 1980; Fujii 1992; Maeda 1994; Fudeyasu and Tsukamoto 2000). The occurrence of a pressure dip is generally only recognized by the analysis of barographic data. Figure 1 shows the time series data of surface wind direction and speed, temperature, dewpoint temperature, and pressure recorded at station K (see Fig. 3)

during the passage of Typhoon Zeb. A pressure dip, consisting of a rapid decrease and subsequent increase in surface pressure, is distinct from the gradual decrease in surface pressure that is recorded during the passage of the typhoon center. Previous studies have shown that pressure dips are meso-β-scale phenomena with a bandlike structure and typical dimensions of 100–200 km by 10–50 km. The maximum observed amplitude of pressure dips is 7–9 hPa, and the duration recorded at a single station is always less than 1 h. Pressure dips are accompanied by strong winds, occasionally causing severe damage at various locations over the Japanese islands. For example, it was reported that extensive damage resulting from instantaneous wind speeds of 54.3 m s^{-1} occurred during a pressure dip associated with Typhoon Mireille (Maeda 1994; Fujita 1992).

The formation mechanism of pressure dips is poorly understood. Matsumoto and Okamura (1985) used Doppler radar data and surface observations to study a

---

* Current affiliation: Japan Agency for Marine-Earth Science and Technology (JAMSTEC), Yokosuka, Japan.

Corresponding author address: H. Fudeyasu, Japan Agency for Marine-Earth Science and Technology (JAMSTEC), 2-15 Natsushima, Yokosuka, Kanagawa 237-0061, Japan.
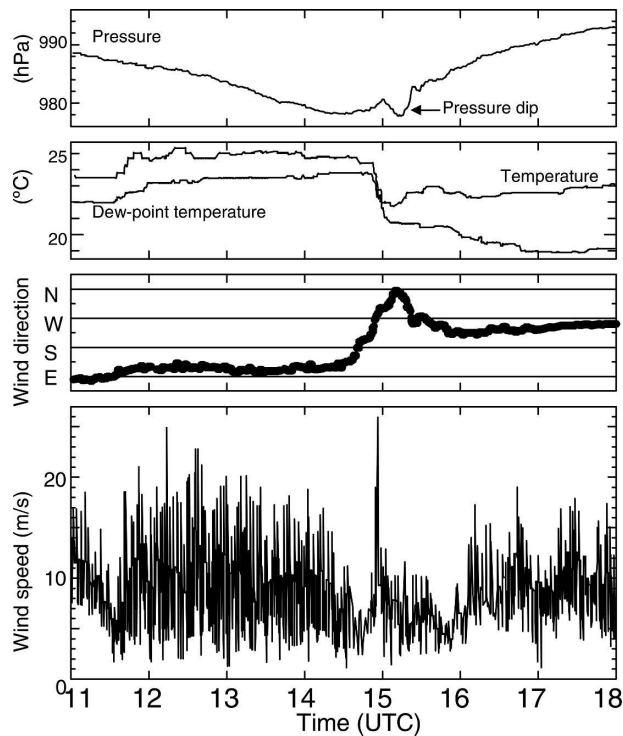E-mail: fudeyasuh@jamstec.go.jp

FIG. 1. The record of the surface pressure, temperature, dew-point temperature, and wind speed and direction as observed at station K from 1100 to 1800 UTC 17 Oct 1998. See Fig. 3 for the location of station K.

pressure dip observed over Japan during the passage of Typhoon Gay and concluded that the pressure dip was due to the passage of an internal gravity wave excited by the convection of the typhoon. Tsujimura (1993) concluded rather that the pressure dip associated with Gay was due to a solitary internal gravity wave. On the other hand, Inoue et al. (1999) argued that the pressure dip observed within Typhoon Zeb was a low pressure region that formed behind the gust front of a gravity current caused by an intense rainband. Thus, it is apparent that the formation mechanism of pressure dips is a controversial issue.

Another controversial issue is the genesis location of pressure dips with respect to the center of the accompanying typhoons. Fujita (1952) described pressure dips on both sides of the movement direction of Typhoon Della at a distance of 50–600 km from the typhoon center. Nakajima et al. (1980) reported pressure dips both ahead of and behind the advancing Typhoon Owen at a distance of 50–100 km from its center. In this case, the pressure dips ahead of the typhoon were short lived and of lesser amplitude than those behind the typhoon. The pressure dips associated with Typhoon Gay and Typhoon Zeb were observed to the left and rear of the northeast-moving typhoons (Matsumoto

and Okamura 1985; Inoue et al. 1999; Fudeyasu and Tsukamoto 2000). The pressure dips that accompanied Typhoon Mireille developed on the rear of the typhoon at a distance of about 200 km from its center (Fujita 1992; Fujii 1992; Maeda 1994).

In this study, we first examined the formation mechanism of pressure dips using a high-resolution numerical model. We focused on the pressure dips associated with Typhoon Zeb because its track was the most suitable for investigating the structure and occurrence of pressure dips because of the availability of comprehensive observational data. The model successfully reproduced the major features of the pressure dip associated with Zeb. We then attempted to clarify the formation mechanism of pressure dips. Another aim of this study was to examine the conditions necessary for the occurrence of pressure dips using the available observational data.

This paper is organized into the following parts. Section 2 describes the observational data and the model used in the study while section 3 compares the simulated pressure dips associated with Zeb with observational data. Additionally, the internal structure of a pressure dip is described. Section 4 examines the formation mechanism of pressure dips. Section 5 presents the features found in observed and simulated pressure dips associated with other typhoons. Section 6 discusses the conditions needed for pressure dip formation while section 7 summarizes the current study.

2. Data and model

a. Data

To identify past occurrences of pressure dips, we analyzed the temporal variations of surface pressure as recorded by the barographs at meteorological stations of the Japan Meteorological Agency (JMA) during the period from 1980 to 1998. The stations are located at approximately 50-km intervals throughout the Japanese islands. We used the following quantitative definitions to distinguish a pressure dip from other features, such as local changes in pressure.

1) The maximum amplitude of the dip in surface pressure observed at each station had to be greater than 1 hPa and had to last for less than 1 h.
2) The pressure dip, as defined in the first definition above, had to be associated with an individual typhoon, and had to be recorded by at least 10 meteorological stations.
3) The movement of the pressure dip, as detected by conditions detailed in the first definition above, had to be recognized in tandem with the movement of the accompanying typhoon.

These quantitative definitions are based on the characteristics of a pressure dip described by Fujita (1952), who stated that a pressure dip is a mesoscale atmospheric phenomenon with a bandlike structure and that the propagation of the pressure dip must be recognized by reference to barographs. The second definition detailed above is required in order to depict the spatial structure of pressure dips. Therefore, in this study, we only considered those pressure dips with significant amplitude and long persistence that were detected over the Japanese islands.

Tracks of typhoons were obtained from the best-track archives of the Regional Specialized Meteorological Centers (RSMC) Tokyo-Typhoon Center. The dataset consisted of the names, positions, maximum surface pressures, and maximum wind speeds of typhoons, generally recorded at 6-h intervals. Estimates of the hourly positions of typhoon centers were determined by linear interpolation based on the 6-h data.

Hourly rainfall patterns were estimated using the Radar-Automated Meteorological Data Acquisition System (AMeDAS) data provided by the JMA. The Radar-AMeDAS data comprise an hourly averaged rainfall analysis created from a composite of observations from operational precipitation radars and the AMeDAS data (Obayashi 1991). The Radar-AMeDAS data during the period from April 1988 to March 2001 have a horizontal resolution of 5 km.

Details of the large-scale atmospheric conditions around the typhoons with pressure dips were reconstructed from the reanalysis data provided by the National Centers for Environmental Prediction–National Center for Atmospheric Research (NCEP–NCAR). The data had been collected every 6 h between 1980 and 1998 with a horizontal resolution of 2.5° (Kalnay et al. 1996). Equivalent black body temperature (T_{BB}) from the Japanese Geostationary Meteorological Satellite spanning the period of 1980–98 was also used.

b. Model

A numerical simulation was performed using the fifth-generation Pennsylvania State University–NCAR Mesoscale Model (MM5), version 3.5. The MM5 is a nonhydrostatic model developed as a community mesoscale model (Dudhia 1993; Grell et al. 1995). The model incorporates multiple nested grids and includes both explicit moist physical processes and cumulus parameterization schemes. This model solves the nonlinear, primitive equations using Cartesian coordinates in the horizontal direction and terrain-following sigma coordinates in the vertical direction. Pressures at the sigma levels were determined from a reference state that was estimated using the hydrostatic equation for
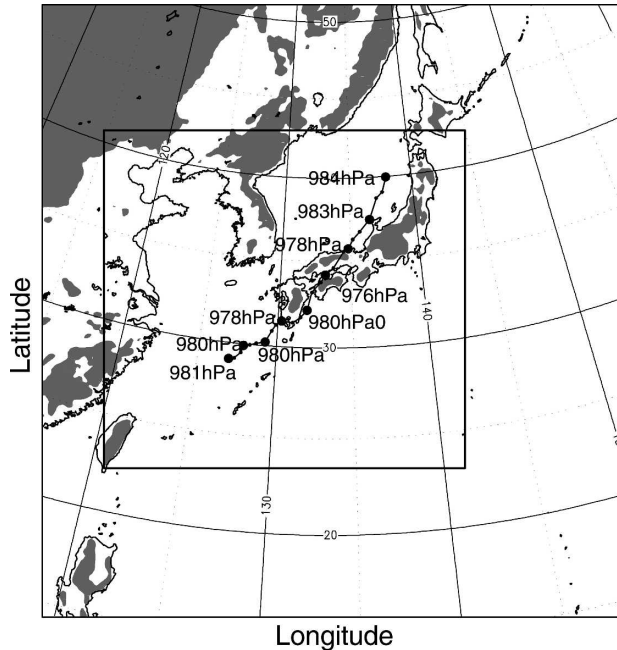

FIG. 2. Model domains of the numerical simulations and terrain. Regions higher than 400 m are shaded. Track (line) and 3-hourly locations (closed circles) of the simulated typhoon derived from the D2 simulation during the period from 0000 UTC 17 Oct to 0000 UTC 18 Oct 1998.

any given sea level pressure and temperature based on a standard lapse rate.

In this study, the model contained 30 sigma levels of fine resolution near the surface, while the top of the model was at 50 hPa. The simulation was conducted using the two domains shown in Fig. 2. The outer domain (D1) had 271 × 271 grid points, centered at 33°N, 133°E, with a horizontal resolution of 15 km. The inner domain (D2) had 460 × 460 points with a horizontal resolution of 5 km. The outer domain was designed to produce the initial and boundary conditions for D2, while D2 was designed to explicitly resolve the fine structures of typhoons and associated pressure dips. We also conducted a simulation using a horizontal resolution of 3 km, but the results were essentially the same as those from the model with a horizontal resolution of 5 km.

A simple ice scheme (Dudhia 1989) was used for the cloud microphysics. In this scheme, cloud water and rainwater below 0°C are treated as ice and snow, respectively. The convective scheme of Grell (1993) was used as a cumulus parameterization only in D1. The model also included the planetary boundary layer (Hong and Pan 1996), a five-layer soil model, and a cloud–radiation interaction scheme (Dudhia 1989, 1993; Grell et al. 1995).

TABLE 1. Summary of initial time and integrated time for simulations.

Typhoon	Domain 0		Domain 1		Domain 2	
	Initial time	Integrated time (h)	Initial time	Integrated time (h)	Initial time	Integrated time (h)
Gay	0000 UTC 21 Oct 1981	48	1800 UTC 21 Oct 1981	30	0000 UTC 22 Oct 1981	24
Wayne	1800 UTC 17 Oct 1989	72	1200 UTC 18 Oct 1989	54	0000 UTC 19 Oct 1989	48
Hattie	0000 UTC 6 Oct 1990	72	1800 UTC 6 Oct 1990	54	0000 UTC 7 Oct 1990	48
Mireille	0600 UTC 26 Sep 1991	48	0000 UTC 27 Sep 1991	30	0000 UTC 27 Sep 1991	30
Oliwa	1200 UTC 14 Sep 1997	72	0300 UTC 15 Sep 1997	57	0600 UTC 15 Sep 1997	54
Vicki	0000 UTC 21 Sep 1998	48	1500 UTC 21 Sep 1998	33	1500 UTC 21 Sep 1998	33

The initial and lateral boundary conditions for D1 in the simulation of Typhoon Zeb were derived from the Global Asian Meteorological Experiment (GAME) reanalysis dataset produced by the Meteorological Research Institute–JMA (see details online at http://gainhub.mri-jma.go.jp/GAME_reanal.html). The dataset includes the 3D analyzed atmospheric fields over the Asian and Pacific regions (80°N–30°S, 30°E–180°), covering the period from April to October 1998. The data have a horizontal resolution of 0.5° for both longitude and latitude, with 17 vertical levels and a 6-h time interval. Sea surface temperature is represented by the skin temperature of the NCEP–NCAR reanalysis dataset (Kalnay et al. 1996).

The simulation of D1 was performed for 42 h, starting at 1800 UTC 16 October 1998, after the model was integrated for 18 h during an initial spinup at 0000 UTC 16 October. During the initial spinup, continuous dynamical assimilation was performed by adding forcing functions to the governing model equations to gradually "nudge" the model state toward the reanalysis data for wind-only components (Grell et al. 1995). The relaxation boundary conditions were adopted as the lateral boundary conditions (Anthes et al. 1987) in which the model-predicted values were relaxed to those estimated from the large-scale analysis data. The D2 simulation began at 0000 UTC 17 October 1998 and was performed for 36 h using the initial and boundary conditions interpolated from the results of the D1 simulation. At the start of the D2 simulation, the center of Typhoon Zeb was located to the southwest of Kyushu, Japan (Fig. 2).

We also used the NCEP–NCAR reanalysis dataset as the initial and lateral boundary conditions in order to simulate other typhoons. This dataset was also used to examine the sensitivity of the conditions used for simulating Zeb. The horizontal resolution of the datasets is coarse in comparison with the GAME reanalysis dataset, and consequently another outer domain (D0) was incorporated into the model in order to nest the simulation of D1. The mesh of D0 had 120×120 points

and a horizontal resolution of 45 km. For the coarse domain D0, the Kuo scheme (Grell et al. 1995) was used as the cumulus convection parameterization, but all other configurations of the model are the same as those used for the D1 simulation. The simulation of D0 was performed using the continuous dynamical assimilation with the typhoon bogus schemes incorporated in MM5. The initial and integration times of all simulations conducted in this study are summarized in Table 1. In the following analysis, we only use the results of D2.

3. The pressure dip associated with Typhoon Zeb

a. Features of the observed pressure dip

Typhoon Zeb was upgraded to a tropical storm (maximum 1-min sustained wind speeds in excess of 17.2 m s^{-1} or 35 kt) from a tropical depression on 11 October 1998 when it was situated at 10°N, 140°E (Fig. 3). The typhoon turned toward the northwest over the vicinity of the Philippine Sea and increased in intensity to that of a super typhoon (maximum 1-min sustained wind speed in excess of 70 m s^{-1} or 135 kt). The typhoon made landfall in Kyushu at 0700 UTC 17 October, with a central pressure of 975 hPa and a maximum wind speed of 25 m s^{-1}. The typhoon then passed over Shikoku and Honshu, the main island of the Japanese islands, at 1400 UTC 17 October. After reaching the Sea of Japan, Zeb moved north-northeast and eventually weakened. It was downgraded to an extratropical cyclone when it was located near Hokkaido at 0000 UTC 18 October.

During the passage of Zeb through the Japanese islands, a considerable decrease and subsequent increase in surface pressure was recorded at several meteorological stations. Figure 4 shows the time series data of surface pressure recorded by barographs at these meteorological stations. In addition to a gradual change in surface pressure related to the passage of Zeb, a sudden 3–8-hPa drop in surface pressure was also discernible. The pressure dips appeared a few hours after the pas-
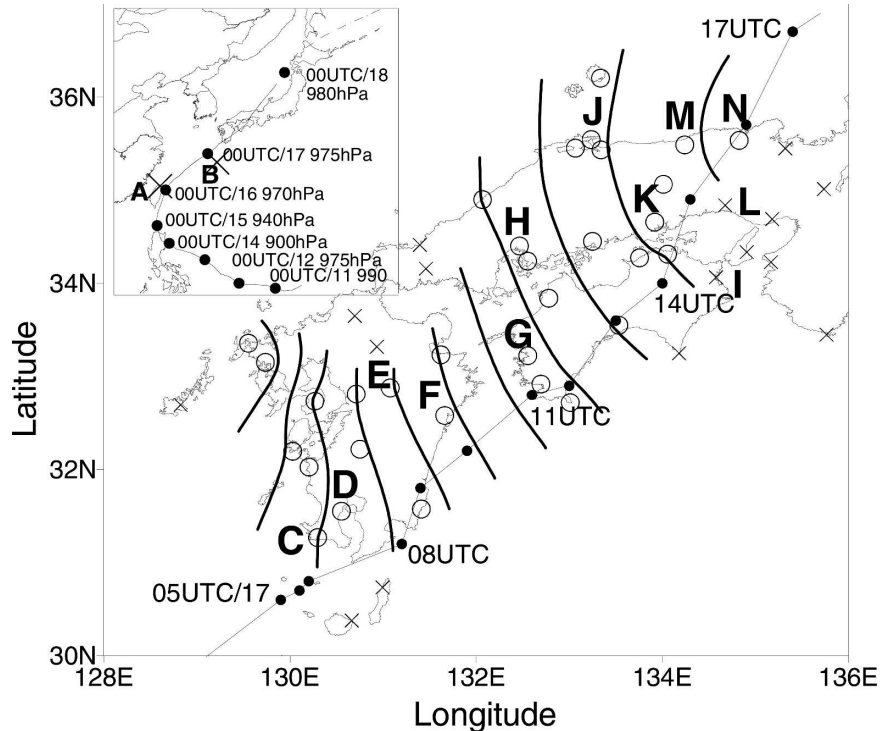
FIG. 3. Hourly locations of pressure dip axis (solid lines) for Typhoon Zeb (black circles). Open circles indicate stations where the pressure dip was observed, whereas crosses indicate stations where the pressure dip was not observed.

sage of the typhoon center for all stations except station J, where a pressure dip was recorded prior to the arrival of the typhoon center. It should be noted that the pressure dip existed only to the northwest of Zeb as it tracked to the northeast (Fig. 3). There is no sign of a pressure dip at stations I and L located to the southeast of the typhoon. A pressure dip was also not observed on the northern part of the Kyushu and Chugoku districts during the period from 0800 to 1200 UTC, indicating that the extent of the pressure dip axis was defined by the isopleths of minimum pressure within the pressure dip. Although most meteorological stations recorded the pressure dips after the passage of the typhoon center, a number of stations far from the typhoon center recorded a pressure dip in advance of the typhoon center during the period from 1300 to 1500 UTC. Station A, located to the northwest of the typhoon track (Fig. 3), recorded no pressure dip. We interpreted this as an indication that the pressure dip axis did not extend to lower latitudes.

To depict the mesoscale structure of the pressure dips, we conducted a time-to-space conversion (TSC) analysis (e.g., Koch and O'Handley 1997). Figure 5 presents the spatial structure of the surface pressure derived from the TSC analysis of surface pressure record-

ings at 28 meteorological stations within a distance of 200 km from the typhoon center between 1400 and 1500 UTC 17 October (see Fig. 3). The surface pressure had an asymmetric distribution. A low pressure region of 100-km length and 20–30-km width extended toward the north-northwest from a point 50 km west of the typhoon center. An area of high pressure to the east of the low-pressure region represented the rise in surface pressure recorded in the time series data immediately prior to the onset of the pressure dip (Fig. 4).

The arrival of the pressure dip was accompanied by a sudden change in surface winds (Fig. 1), although these wind changes were not observed at all meteorological stations because of local effects, such as mountainous terrain. Wind speeds weakened after the passage of the typhoon center, but strong winds were observed immediately prior to the arrival of the pressure dip. Station K was located to the left-hand side of the moving direction of Zeb and would therefore be expected to record an anticlockwise change in wind direction with the passing of the typhoon. The wind direction, however, recorded a clockwise change for the 30 min prior to the arrival of the pressure dip.

The approach of the pressure dip was also accompanied by rapid changes in surface temperature and dew-
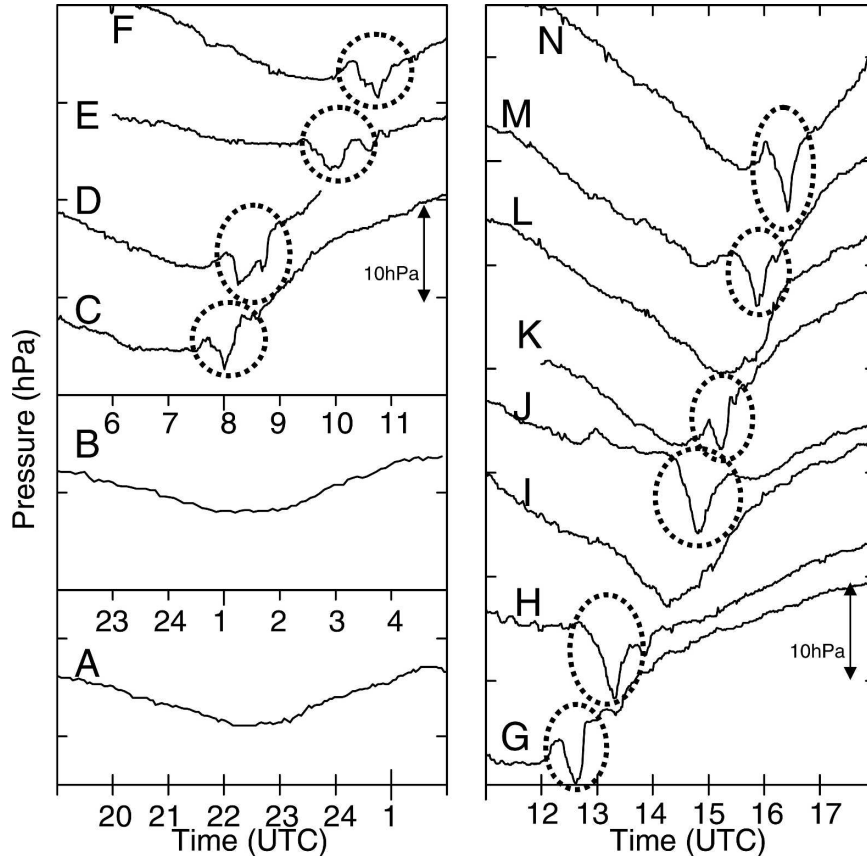
FIG. 4. Barographic charts recorded at meteorological stations during the passage of Typhoon Zeb from 16 to 17 Oct 1998. Station locations are indicated in Fig. 3. The detection of a pressure dip at each station is indicated by a dashed circle.

point temperature, which fell 3°C one hour before the pressure dips appeared (Fig. 1). These trends were only observed at stations near the track of the typhoon. Temperature changes are related to surface fronts associated with Zeb, rather than the pressure dip itself (see Fig. 22). In fact, Fujita (1952) documented no significant change in surface temperature associated with a pressure dip. However, a few hours before a pressure dip appeared, a sudden decrease in surface temperature and dewpoint temperature was recorded at some meteorological stations (see also Fig. 1 of Fujita 1952, Fig. 4 of Matsumoto and Okamura 1985, Fig. 3 of Fujii 1992, and Fig. 2 of Maeda 1994). As stated above, these changes in temperature appear to be related to fronts associated with the typhoons rather than the pressure dip. This topic will be discussed later in more detail.

Figure 6 shows the hourly rainfall amount derived from the Radar-AMeDAS data at 0700, 0900, 1300, and 1500 UTC 17 October 1998. Intense rainfall precedes the arrival of the pressure dip axis. The rainfall was weak at the center of the pressure dip and stopped with the passing of the pressure dip axis. The AMeDAS data, which contain a record of surface wind, temperature, and rainfall averaged over 10-min intervals since 1995, show that rainfall changes occurred abruptly over a period of less than 30 min (not shown).

b. Validation of simulated pressure dip

In this section, we validate the features of the Typhoon Zeb simulation. The track of Zeb simulated in D2 with the finest resolution, determined from the area of minimum sea level pressure of the simulated typhoon, is shown in Fig. 2. The simulated typhoon track is generally in good agreement with the observed typhoon track (Fig. 3). The central pressure of the simulated typhoon are about 980 hPa on 17 October when the typhoon passed over Kyushu, Shikoku, and Honshu before reaching the Sea of Japan. The recorded pressures within the center of Zeb at this time were in the range 975–980 hPa. The track of the simulated typhoon, however, is delayed by an hour in comparison with the actual movement of Zeb. This is because the initial
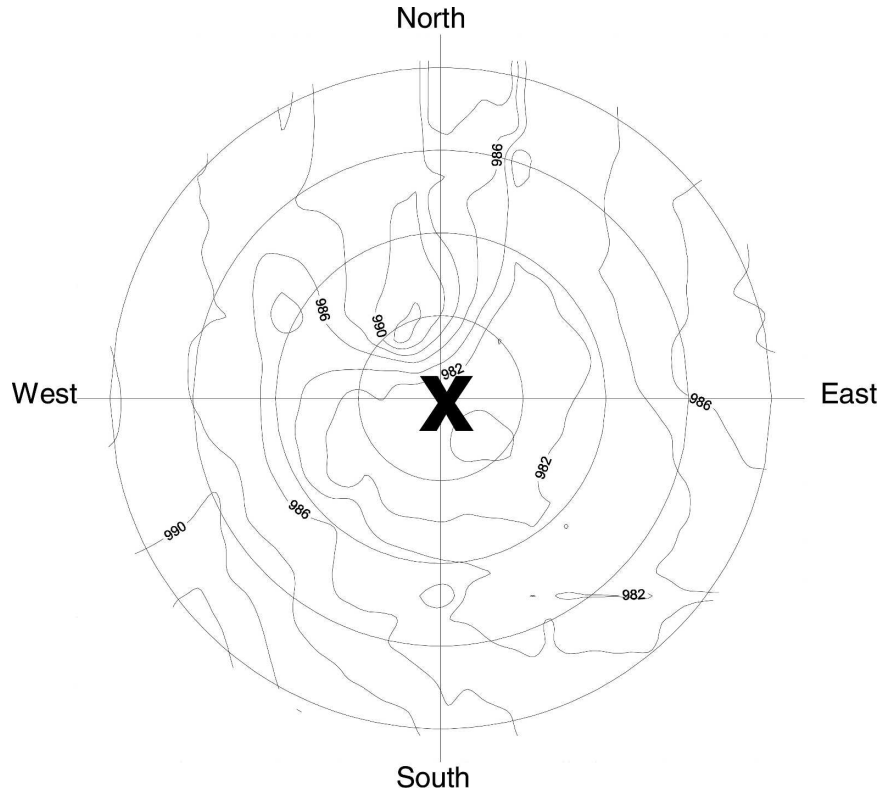
FIG. 5. Sea level pressure field for Typhoon Zeb during 1400–1500 UTC derived by a TSC analysis. Contour interval is 2 hPa. The cross represents the position of the typhoon center.

position of D2 shifted westward because of the insufficient simulation of D1, which had a coarse resolution. This discrepancy may be related to a bias in the boundary conditions or in the assimilation used in the present model. Although the arrival time of the simulated typhoon differs from actual observations, the track and intensity of Typhoon Zeb are well reproduced by the model.

Next, we compared the simulated pressure dips with those observed within Zeb. Figure 7 presents the time series data of the simulated sea level pressure at 3-min intervals at each station (see Fig. 3). Portions of the time series data at stations A and B are not shown because the typhoon center had passed over these stations prior to the initial time of the D2 simulation at 0000 UTC 17 October (Fig. 2). Of note, the locations of stations H, I, J, K, L, M, and N have been shifted 1° westward from their actual locations to accommodate differences between the simulation and observational data for the period after Zeb made landfall over Shikoku.

The time series data of simulated sea level pressure record a diplike decrease in sea level pressure associated with the passage of the typhoon center, although their amplitudes are generally smaller than the observed amplitudes (Fig. 4). The peak of the pressure dip

was recorded at station C at 0900 UTC, station D at 0955 UTC, station E after 1050 UTC, station F at 1115 UTC, and station G at 1355 UTC. The pressure dips generated within the simulation occur about an hour after the observed pressure dips were recorded at each station. This time discrepancy occurs because the track of the simulated typhoon was 1 h late compared with the actual track of Zeb (Figs. 2 and 3). A pressure dip of 4.5 hPa was recorded at station H at 1325 UTC, and pressure dips were also recorded at station J at 1445 UTC and station K at 1515 UTC. These times are comparable to the timing of the actual pressure dips observed at each station. As in the observational data, there is no sign of a pressure dip at stations I and L. In contrast to the observational data, the simulated pressure dip was not recorded at stations M and N, although the reason for this is not clear.

Figure 8 shows the time sequence data of the simulated sea level pressure from 0500 to 1800 UTC 17 October 1998 together with the simulated hourly rainfall. At 1300 UTC when the typhoon center was located over western Shikoku (Fig. 8d), a low pressure region distinct from the typhoon center extended toward the north from an area west of the typhoon center. This low pressure region corresponded to the pressure dip axis,
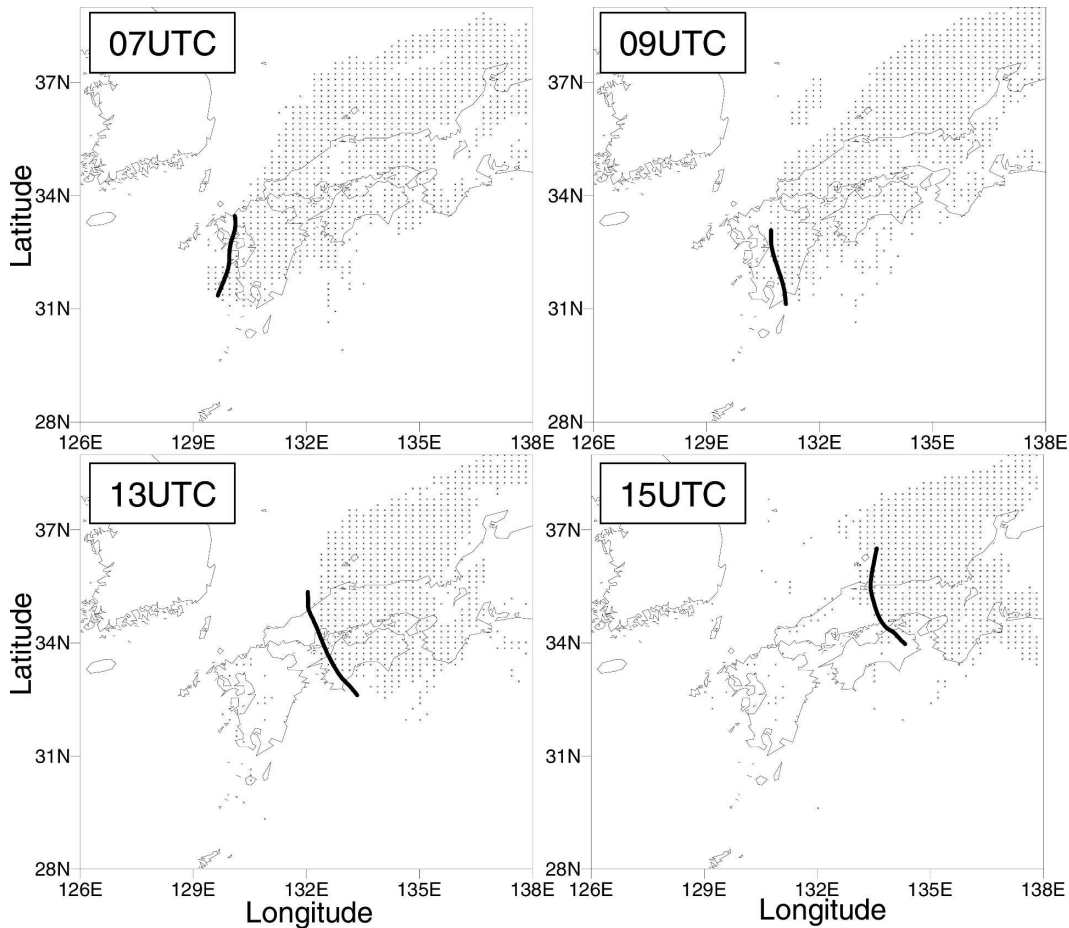
FIG. 6. Hourly rainfall region of more than 1 mm h^{-1} derived from the Radar-AMeDAS data and the pressure dip axis at 0700, 0900, 1300, and 1500 UTC 17 Oct 1998. The solid lines denote the location of the pressure dip axis.

as defined by isopleths of the minimum pressure within the pressure dip. The passage of the pressure dip axis can be traced by a sudden decrease and then increase in the simulated sea level pressure recorded at several stations (Fig. 7). The pressure dip has a length of 200 km and a width of 10–30 km, which is consistent with the dimensions derived from observational data (Fig. 5). It should also be noted that as in the actual situation (Fig. 6), rainfall precedes the arrival of the simulated pressure dip axis. The simulated rainfall is weak at the center of the pressure dip and ceases with the passage of the pressure dip axis, which is consistent with the rainfall features observed (Fig. 6).

The simulated pressure dip was not recorded before 0500 UTC (Fig. 8a) but developed in the northwest quadrant of the typhoon after 0800 UTC (Fig. 8b) when the typhoon center was located over the sea to the southwest of Kyushu. This indicates that the formation of the pressure dip is not related to the topography of the Japanese islands (Fig. 2). The pressure dip axis then

moved northeastward with the typhoon and extended to an area west of the typhoon center (Fig. 8c). The pressure dip was most clearly discernible at 1300 UTC (Fig. 8d). As the typhoon moved farther northeast, the pressure dip broke down (Figs. 8e,f) and was not recorded at stations M and N (Fig. 7).

Although the amplitude of the simulated pressure dips was weaker than that of the observed dips, the features of the simulated pressure dips were sufficiently similar to those of the observed pressure dips that we could confidently use the simulation data to investigate the formation mechanism of pressure dips.

c. Structure of the simulated pressure dip

Figure 9 shows the vertical sections of the potential temperature anomaly at each pressure level across station H at 1300 UTC (see Fig. 8d) together with the sea level pressure. The potential temperature anomaly was calculated as the deviation from the average potential temperature of the entire D2 area. The upper tropo-
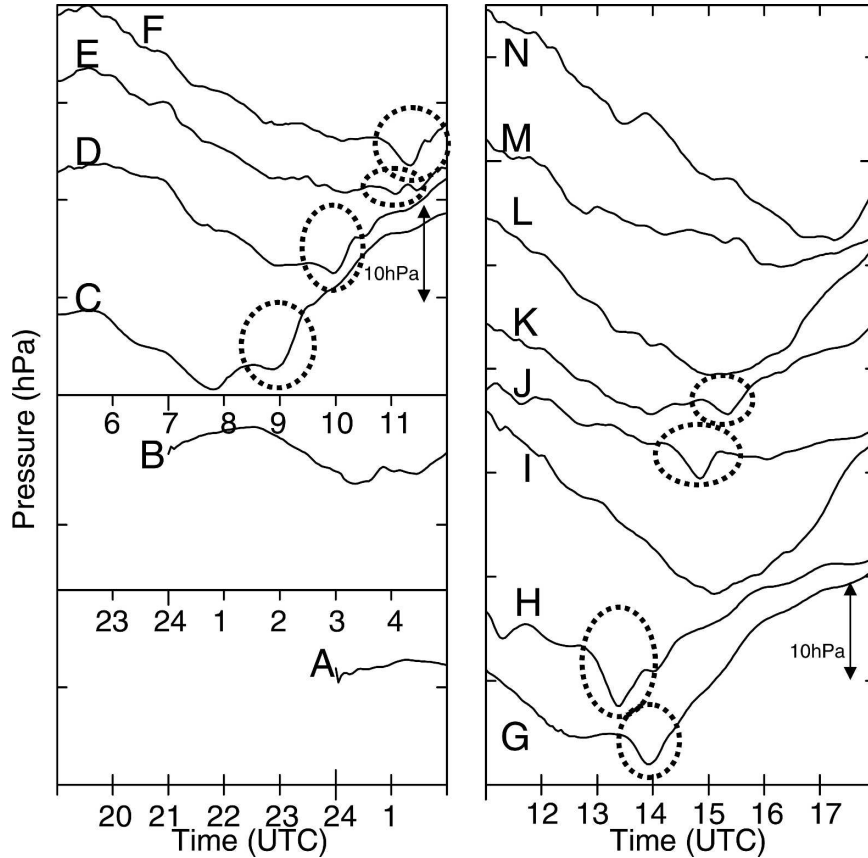
FIG. 7. Simulated time series data of the sea level pressure for meteorological stations during the passage of a typhoon from 16 to 17 Oct 1998. Station locations are indicated in Fig. 3. The detection of a pressure dip at each station is indicated by a dashed circle.

sphere contains warm anomalies associated with the warm core of the typhoon that result in a broad lowering in sea level pressure. In the troposphere below 700 hPa, warm potential temperature anomalies existed east of 132°E because of a northward warm advection associated with cyclonic circulation, while the anomalies were relatively cool to the west of 132°E. The low-level front at 132°E was consistent with the changes in surface temperature observed prior to the pressure dip, which were related to fronts associated with the typhoons rather than the pressure dip. At 131.5°E in the lower troposphere, within the colder region of the low-level front at 132°E, there were remarkable warm potential temperature anomalies from 700 to 900 hPa that corresponded to a dip in sea level pressure.

Here we use the warm potential temperature anomalies, assuming a hydrostatic balance, as a tool to estimate the magnitude of the pressure dip. The hypsometric equation is written as follows:

$$\Delta z = z_2 - z_1 = \frac{R\overline{T}}{g} \ln\left(\frac{p_1}{p_2}\right) \quad (z_1 < z_2, p_1 > p_2), \quad (1)$$

where p is the pressure (Pa), z is the height (m), g is the acceleration due to gravity (m s^{-2}), R is the universal ideal gas constant, and $\overline{T}$ is the mean temperature (K) of the layer of thickness Δz. The anomalous temperature ΔT is measured as the deviation from the mean temperature $\overline{T}$ and determines the pressure $p_1 + \Delta p$ as follows:

$$\ln(p_1 + \Delta p) = \frac{\overline{T}}{\overline{T} + \Delta T} \ln\left(\frac{p_1}{p_2}\right) + \ln p_2. \quad (2)$$

Under the conditions described in Fig. 9, $\overline{T} = 310$ K, $p_1 = 900$ hPa, $p_2 = 700$ hPa, and $\Delta T = 5.0$ K, which makes $\Delta p = -3.8$ hPa. This estimate of the pressure decrease within pressure dips is comparable to the simulation value of about 4.5 hPa, suggesting that the warm potential temperature anomalies in the lower troposphere are the major cause for the formation of pressure dips.

Figure 10 shows the vertical sections of vertical velocity, relative humidity with winds in the plane, cloud water/ice mixing ratio, and rainwater/snow mixing ra-
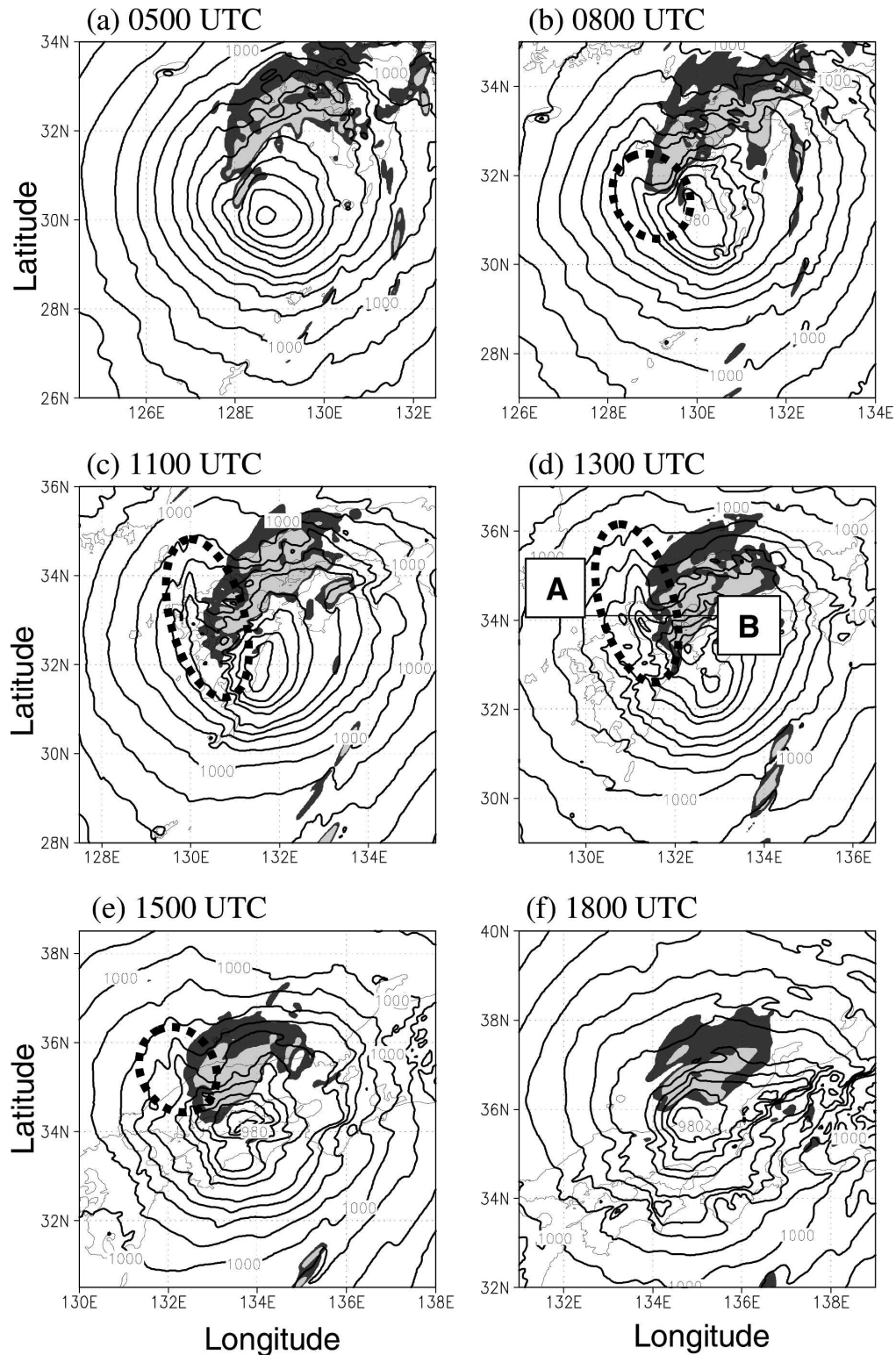
FIG. 8. Simulated sea level pressure fields and hourly rainfall within D2 at (a) 0500, (b) 0800, (c) 1100, (d) 1300, (e) 1500, and (f) 1800 UTC 17 Oct 1998. Contour interval is 2 hPa. The detection of a pressure dip is indicated by a dashed circle. Regions of rainfall of 10–20 mm h^{-1} are heavily shaded while regions with greater than 20 mm h^{-1} are lightly shaded.
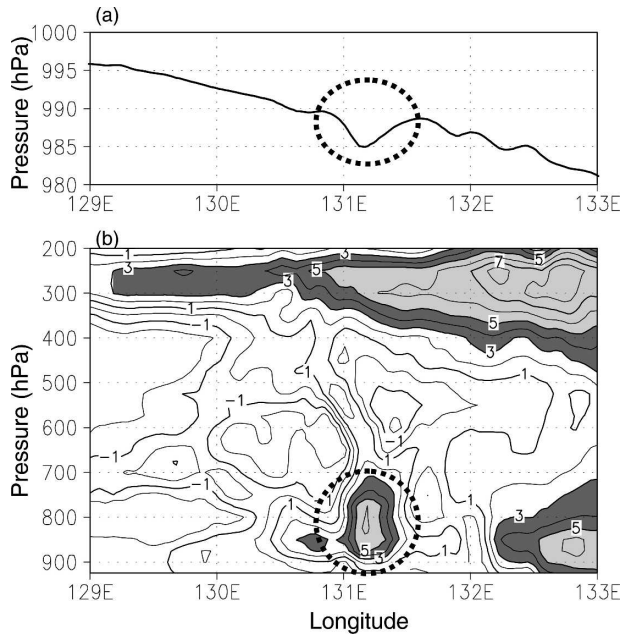
FIG. 9. Cross section of (a) sea level pressure and (b) potential temperature anomalies at 1300 UTC 17 Oct 1998. Location of cross section is indicated by the line A–B in Fig. 8d, at the latitude of 34.1°N. Contour interval is 1 K. Regions with anomalies of 3–5 K are heavily shaded while those greater than 5 K are lightly shaded. The detection of warm potential temperature anomalies related to a pressure dip is indicated by a dashed circle.

tio. Near the typhoon center, there is a relatively moist region accompanied by strong ascending flow throughout the entire troposphere (Figs. 10a,b). Over the pressure dip region immediately west of the ascending flows, there is a locally strong descending flow from 300 hPa down to the surface, which is accompanied by a wavelike vertical circulation to the west. In association with the strong descending flow, there is the relatively dry region below 600 hPa in the same narrow region as the warm potential temperature anomalies. The dry region is connected with a dry region in the upper and middle troposphere and is accompanied by the westerly winds.

At higher altitude, ice was advected outward from the typhoon center, forming the overhanging anvil over the pressure dip region (Fig. 10c). This ice water in the anvil aggregated and transformed into snow as it approached the 0°C level (Fig. 10d). It should be noted that in the present simulations, cloud water and rainwater below 0°C are treated as cloud ice and cloud snow in the cloud microphysics (Dudhia 1989). Therefore, when cloud snow fell through the 0°C level, it melted and fell to the ground as rain. The change in fall velocities from snow to rain caused the concentrations of water content to be larger above the melting level

than below the melting level. The pressure dip was found below the overhanging anvil. These images imply that the pressure dip is linked to warm potential temperature anomalies in the lower troposphere, accompanied by the intrusion of an upper dry air mass caused by a locally strong descending flow.

The descending flow area is found along the confluence zone resulting from the interaction between the typhoon's circulation and the environmental westerly winds when the typhoon enters the zone of midlatitude westerlies (Fig. 11). The inflow of a dry air mass by the midlatitude westerlies into the moist area of the typhoon induces a frontal zone of equivalent potential temperature in the middle troposphere. At the beginning of the simulation, the confluence zone accompanied by descending airflow existed far to the north of the typhoon (Figs. 11a,b). As the typhoon moved northeastward, the confluence and descending airflow intensified at the rear of the typhoon (Figs. 11c,d). As the typhoon continued to move still farther northeastward, the confluence to the rear of the typhoon rapidly became weaker and the descending airflow disappeared (Figs. 11e,f). Therefore, the occurrence of the simulated descending flow area seems to be related to the evolution of the interaction between the typhoon's circulation and midlatitude westerlies.

4. Formation mechanisms of the simulated pressure dip

a. Heat budget

We will now consider how the warm potential temperature anomalies in the lower troposphere form. The process of anomaly formation can be investigated by describing the anomalies in terms of a thermodynamic equation. The time tendency of potential temperature is estimated by the difference in the potential temperature sampled at a time interval of 3 min. The diabatic term, including radiation, diffusion, and net heating related to phase changes of water, is defined as the residual derived from both the horizontal and vertical advection terms and the time tendency.

Figure 12 displays the time series data of the potential temperature anomalies, which are calculated as the deviation of temperature at a point from the average temperature over the D2 area at sea level pressure. Data were calculated at each pressure level over station H (Fig. 3), where the largest dip in pressure was detected (Fig. 7). During the period from 0700 to 1500 UTC, sea level pressure decreased in association with the passage of the typhoon (Fig. 12a). This decrease in surface pressure was related to the warm core in the upper troposphere (Fig. 12b). The decrease due to the
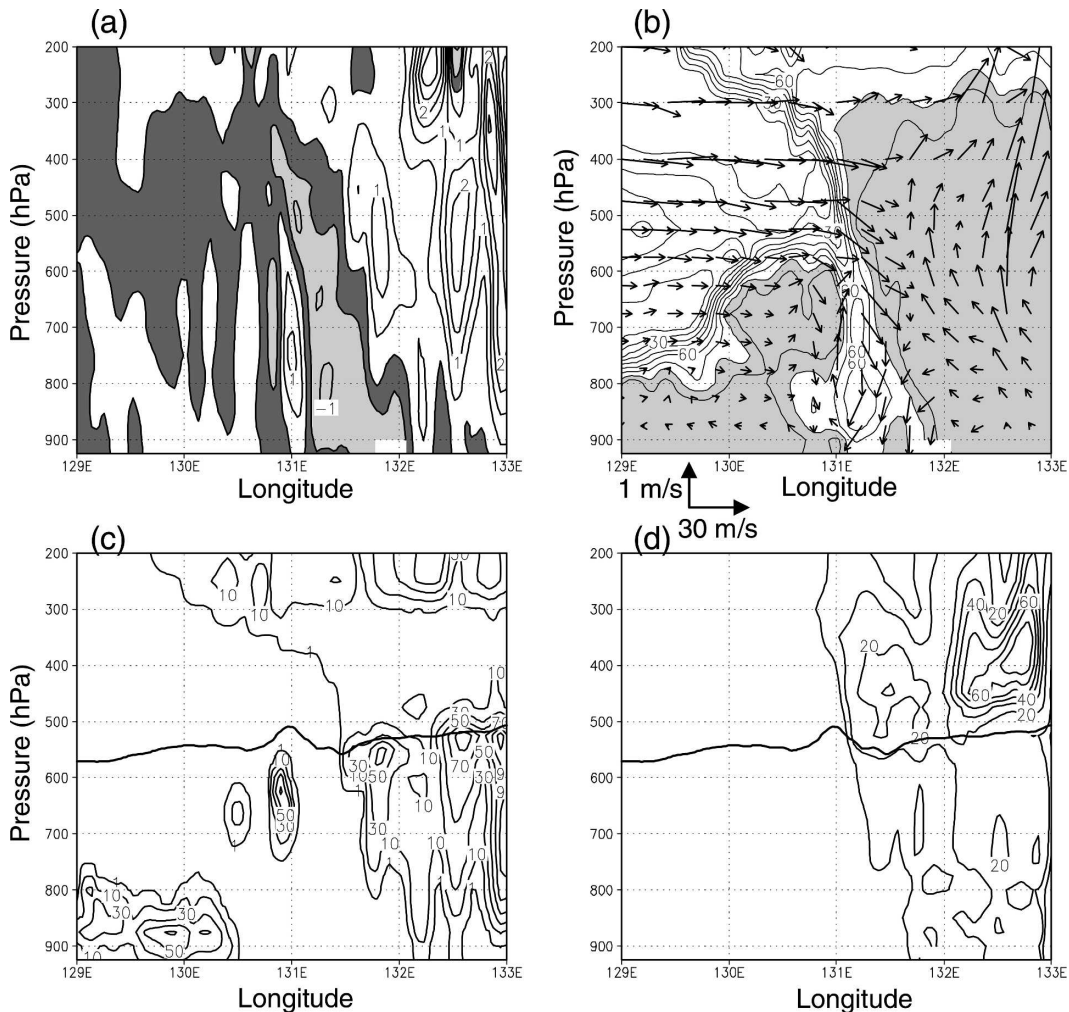
FIG. 10. Same cross-sectional profiles as in Fig. 9 but for (a) vertical velocity, (b) relative humidity and the zonal and vertical components of the winds (m s^{-1} arrows, scale at bottom left), (c) cloud water/ice mixing ratio, and (d) rainwater/snow mixing ratio. Contour interval in (a) is 0.5 m s^{-1}. Dark shading represents areas with vertical velocity less than 0.0 m s^{-1} while light shading represents areas of vertical velocity less than −0.5 m s^{-1}. Contour interval in (b) is 10% and the regions greater than 80% are shaded. Contour interval in (c) is 2.0 × 10^{-5} kg kg^{-1} and in (d) is 1.0 × 10^{-3} kg kg^{-1}. The solid lines indicate the level of 0°C.

pressure dip appeared at station H from 1245 to 1325 UTC, coinciding with the development of warm potential temperature anomalies in the lower troposphere. The thermodynamic balance showed that the warming in the lower level from 1315 to 1330 UTC was caused mainly by vertical advection (Fig. 13). Although the cooling due to the diabatic term contributed partly to counteracting the warming, the adiabatic warming of the descending air in the lower level was not balanced by diabatic cooling. The cooling due to the horizontal advection term accompanied by the cyclonic circulation was relatively small in the lower level. This indicates that the adiabatic descent of air is responsible for the formation of warm potential temperature anomalies in

the lower troposphere. However, at a level above 600 hPa, warming due to vertical advection was balanced by the diabatic term. Warming at 400 hPa resulted from the outflow of warmer air from the typhoon center, while cooling at 550 hPa seemed to be related to the inflow of environmental air with a lower potential temperature caused by the westerlies.

b. Trajectory analysis

To further clarify the formation of the warm potential temperature anomalies in the lower troposphere, we conducted a backward trajectory analysis using 3D winds sampled at 3-min intervals. Initially, 80 parcels were uniformly defined in the 700-hPa level over
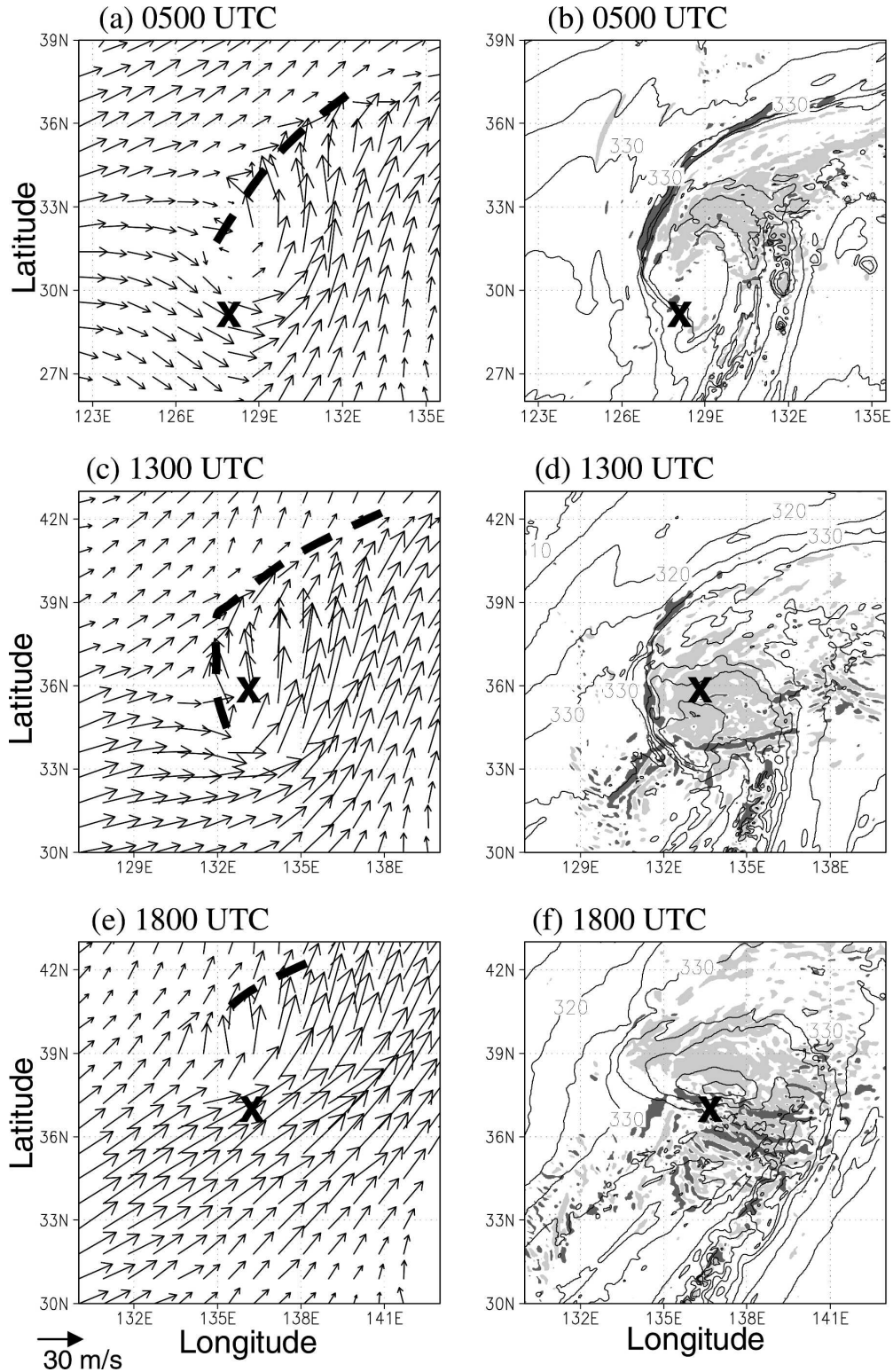
FIG. 11. Winds (m s^{-1} arrows, scale at the bottom left) at 500 hPa for (a) 0500, (c) 1300, and (e) 1800 UTC 17 Oct 1998. (b), (d), (f) Same as in (a), (c), (e) but for equivalent potential temperature and vertical velocity. Regions larger than 0.2 m s^{-1} are lightly shaded while regions smaller than −0.2 m s^{-1} are heavily shaded. Contour interval of equivalent potential temperature is 10 K. Solid broken lines indicate the confluence zone between the typhoon's circulation and the midlatitude westerly winds while crosses represent the position of the typhoon center.
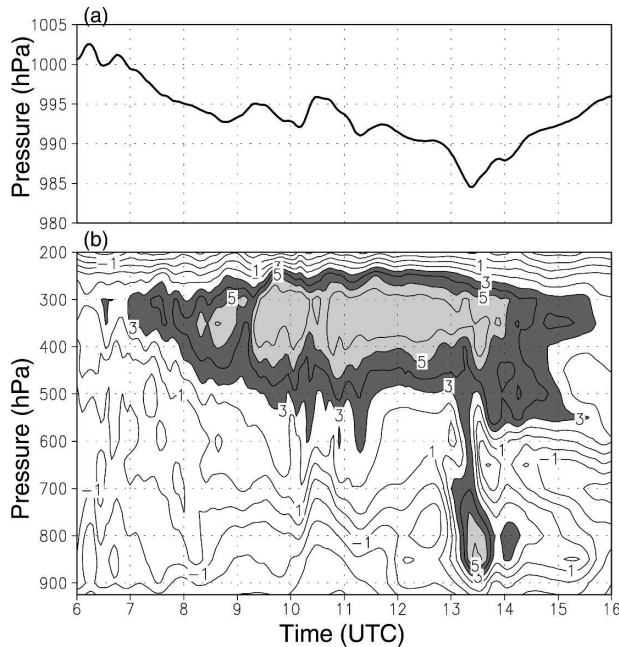
FIG. 12. Time series data of (a) sea level pressure and (b) anomalies of potential temperature at station H for the period 0600–1600 UTC 17 Oct 1998. Contour interval is 1 K. Dark shading indicates areas with an anomaly of 3–5 K while light shading indicates areas with anomalies greater than 5 K.
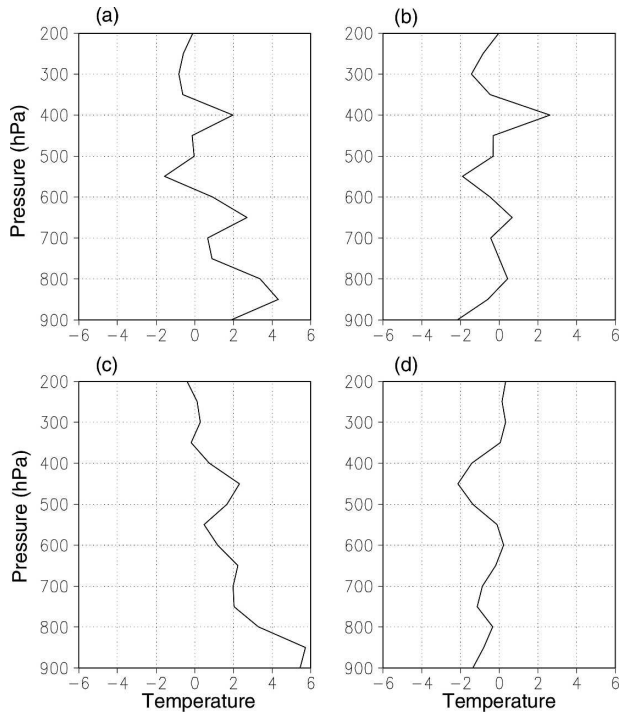

FIG. 13. Vertical profiles of (a) time tendency of potential temperature, (b) horizontal advection, (c) vertical advection, and (d) diabatic effect at station H for the period 1315–1330 UTC 17 Oct 1998.

the surrounding area of station H (34.0°–34.7°N, 131.5°–132.0°E) at 1300 UTC. This region includes both the pressure dip axis and surrounding areas. Figure 14 shows the trajectories of the parcels over 12 h between 0100 and 1300 UTC. The origins of the parcels that resided over the pressure dip can be traced back in time to the eastern coast of China (Fig. 14a), while the parcels in the surrounding area originated from the east-northeast and, to a lesser degree, from the south (Fig. 14b).

Figure 15 presents the time series data of several averaged quantities of parcels that originated from the west (western parcels), which were initially released at the 700-hPa level over the surrounding area of station H. Also shown in the figure are the time series data of parcels that originated from the east-northeast (eastern parcels), which were initially situated slightly east of station H. In the colder region over the northern coast of Honshu, the eastern parcels remained below 3000 m until 1000 UTC (Figs. 14b and 15a). At 1000 UTC, the eastern parcels were brought into the typhoon center and ascended to 3000 m. The potential temperature and equivalent potential temperature increased with the moist-adiabatic lapse rate (Fig. 15b).

The western parcels could be traced back to the upper level around 10 000 m (above 300 hPa) at 0100 UTC

(Fig. 15a). Up until 1030 UTC, strong upper-level westerly winds propelled the western parcels to the east-northeast (Fig. 14a) on the gently descending slope of the isentropic surface within the upper troposphere. The western parcels conserved potential temperature and equivalent potential temperature (Fig. 15b) and subsequently had low humidity (Fig. 15d). The initial motion of the western parcels was thus predominantly adiabatic. Once the western parcels had overtaken the northeastward-moving typhoon between 1030 and 1300 UTC, they moved rapidly downward from 8000 to 3000 m within the intense descending flow (Figs. 15a,c). During this period, the water mixing ratio of the western parcels increases along with relative humidity (Fig. 15d), indicating that water was supplied from the moist region of the typhoon. Although the mixing ratio of the western parcels increased, the equivalent potential temperature remained steady as the potential temperature decreased from 1030 to 1200 UTC (Fig. 15b). From 1245 to 1300 UTC, when the pressure dips began to appear in the vicinity of station H, the changes in potential temperature, humidity, and water mixing ratio were small, suggesting that evaporative cooling was insufficient to offset adiabatic warming because there were fewer hydrometeors below the melting level.
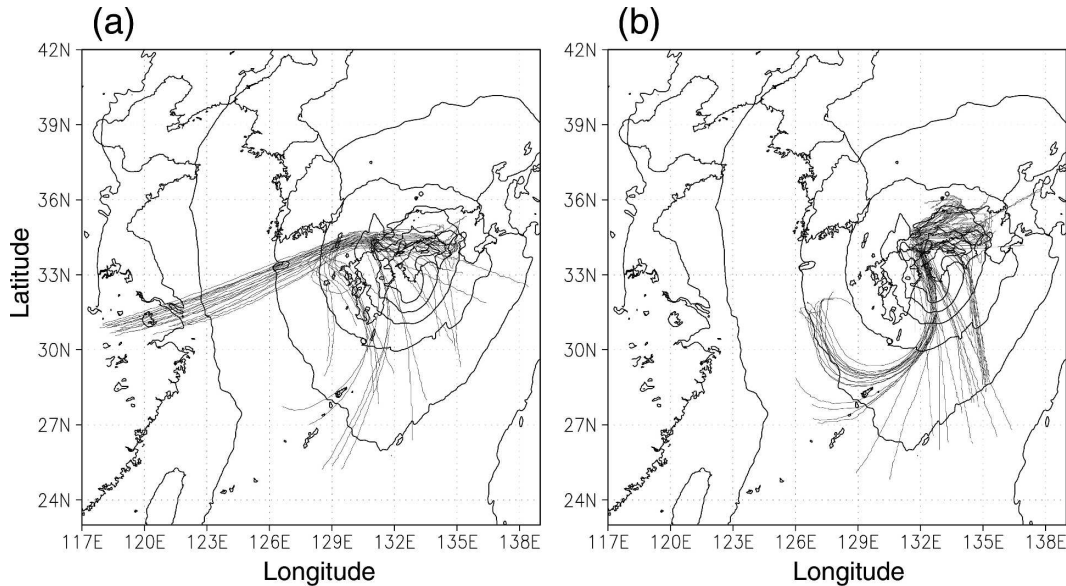
FIG. 14. Trajectories of 80 parcels over 12 h between 0100 and 1300 UTC 17 Oct 1998. The origins of the parcels are at the 700-hPa level over the (a) pressure dip axis and (b) surrounding areas.

Thus, the western parcels were warmer by 4 K than the eastern parcels (Fig. 15b).

The above trajectory analysis suggests that downdrafts play an important role in the formation of pressure dips. As a typhoon moves into the midlatitude westerlies, dry air associated with the westerlies enters the typhoon, which contains saturated air. The interaction between the typhoon's circulation and the westerly winds forms equivalent potential temperature fronts at the midlevel, while an overhanging anvil is evident at the upper level. Next, dry air entering just below the anvil is cooled by evaporation and sublimation (Figs. 15b,d), causing it negative buoyancy (Fig. 15f), hence producing downdrafts (Fig. 15c). Thus, the formation of a mesoscale downdraft results from the cooling of evaporation and sublimation related to dry air masses carried by the upper-level westerly winds toward the moist typhoon region. The downdraft peaked at 1215 UTC (Fig. 15c), when the parcels reached the melting level (Figs. 10c,d). These parcels underwent accelerated evaporation and melting until they passed through the melting level. After passing the melting level, evaporative cooling became insufficient to offset adiabatic warming because there was an insufficient amount of water in the lower level (Figs. 15e,f). As a result, warm potential temperature anomalies appeared in the lower level, causing a pressure dip. The horizontal scale of pressure dips was determined by the width of the region of mesoscale downdrafts that occurred around the melting level. Warming in the lower levels gave the parcels positive buoyancy (Fig. 15f), resulting in the deceleration of downdrafts (Fig. 15c). It should be noted that the downdraft impinging on the lower levels excited gravity waves on the rear side (Figs. 10a,b), but the induced surface pressure change was much weaker than that caused directly by the downdrafts (Fig. 9).

5. Pressure dips associated with other typhoons

a. Features of observed pressure dips

In the previous sections, we described the characteristics of pressure dips observed during the passage of Zeb. Here we describe the general characteristics of pressure dips. During the period from 1980 to 1998, 89 tropical cyclones of at least tropical storm intensity passed across Japan or moved along the southern coast of Japan. Seven of these typhoons were accompanied by pressure dips. A greater proportion of the typhoons may have been accompanied by pressure dips, but such dips in typhoons (whose tracks are at sea, far from the Japanese islands) could not be detected. Furthermore, our definitions excluded pressure dips with a small amplitude and short persistence. The characteristics of each pressure dip and typhoon are summarized in Table 2, while the typhoon tracks and locations of the pressure dip axis defined by the isopleths of minimum pressure within the pressure dip are shown in Fig. 16. All of these typhoons had considerable intensity with central pressures below 980 hPa at the time they approached the Japanese islands (Table 2). They moved quickly toward the northeast or north-northeast during their passage over the Japanese islands, weakened rap-
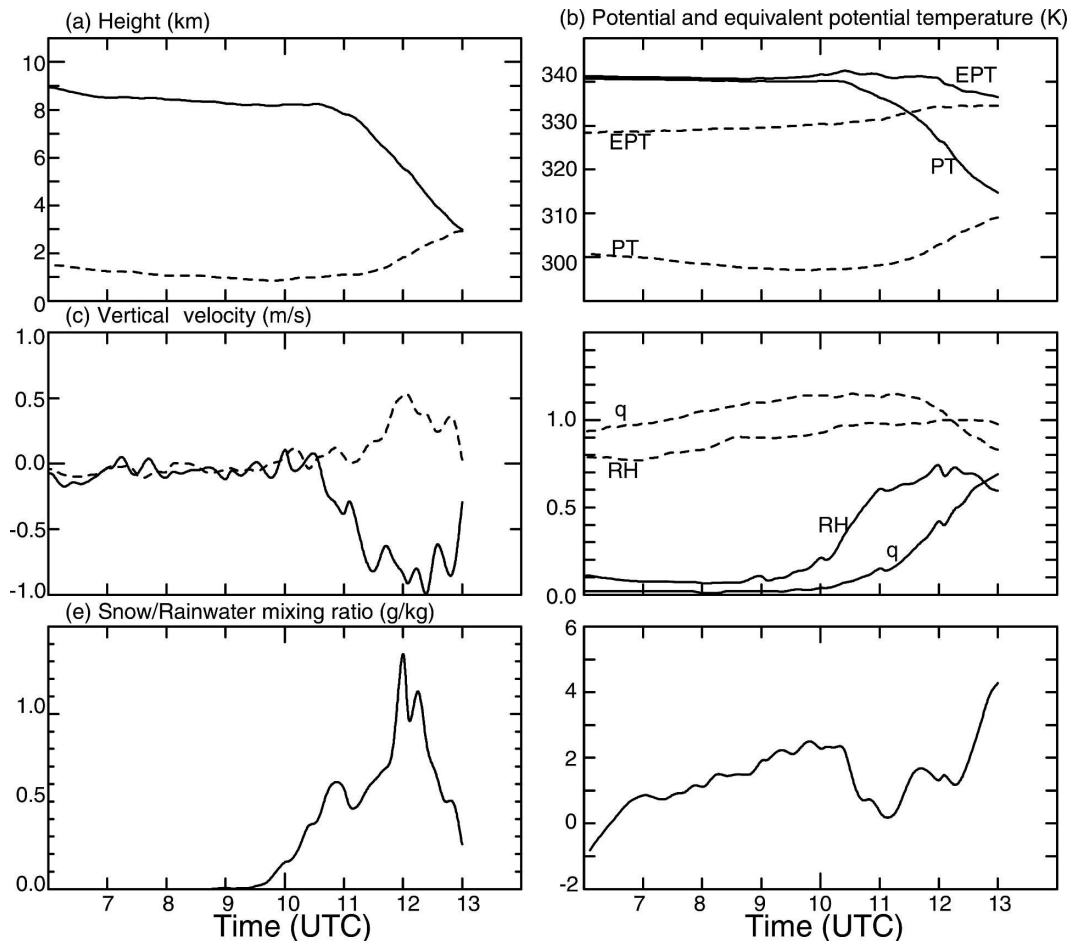
FIG. 15. Time series data of several averaged parameters of the western (solid line) and eastern (dashed line) parcels over 12 h between 0100 and 1300 UTC 17 Oct 1998: (a) height, (b) potential temperatures and equivalent potential temperatures, (c) vertical velocity, (d) water vapor mixing ratio and relative humidity, (e) rainwater/snow mixing ratio, and (f) the anomalies of potential temperature.

idly, and eventually transformed into extratropical cyclones.

Typhoon Gay approached near Tokyo on 22 October 1981 without making landfall (Fig. 16a). At that time, the pressure dip axis extending to the north and south was recorded along the southern coast of Honshu. Typhoon Wayne moved along the southern coast of the Japanese islands from 19 to 20 September 1989 (Fig. 16b). The pressure dip axis related to the movement of the typhoon was observed in Kyushu and along the southern coast of Shikoku. Typhoon Hattie accelerated northeastward along the coast of the Japanese islands

TABLE 2. Summary of the features of the detected seven typhoons with pressure dips.

| Typhoon	Landfall date	Central pressure at landfall (hPa)	Movement speed at 32°N (km h^{-1})	No. of stations that observed dip	Max amplitude of dip (hPa)	Avg amplitude of dip (hPa)	Length of dip axis (km)
Gay	22 Oct 1981	965	40	21	9	4.2	150
Wayne	19 Sep 1989	975	25	14	7	2.4	100
Hattie	8 Oct 1990	975	25	30	5	2.5	100
Mireille	27 Sep 1991	940	45	18	6	2.7	150
Oliwa	16 Sep 1997	965	35	15	5	2.1	100
Vicki	22 Sep 1998	960	50	13	4	1.9	150
Zeb	17 Oct 1998	980	20	28	8	3.9	150
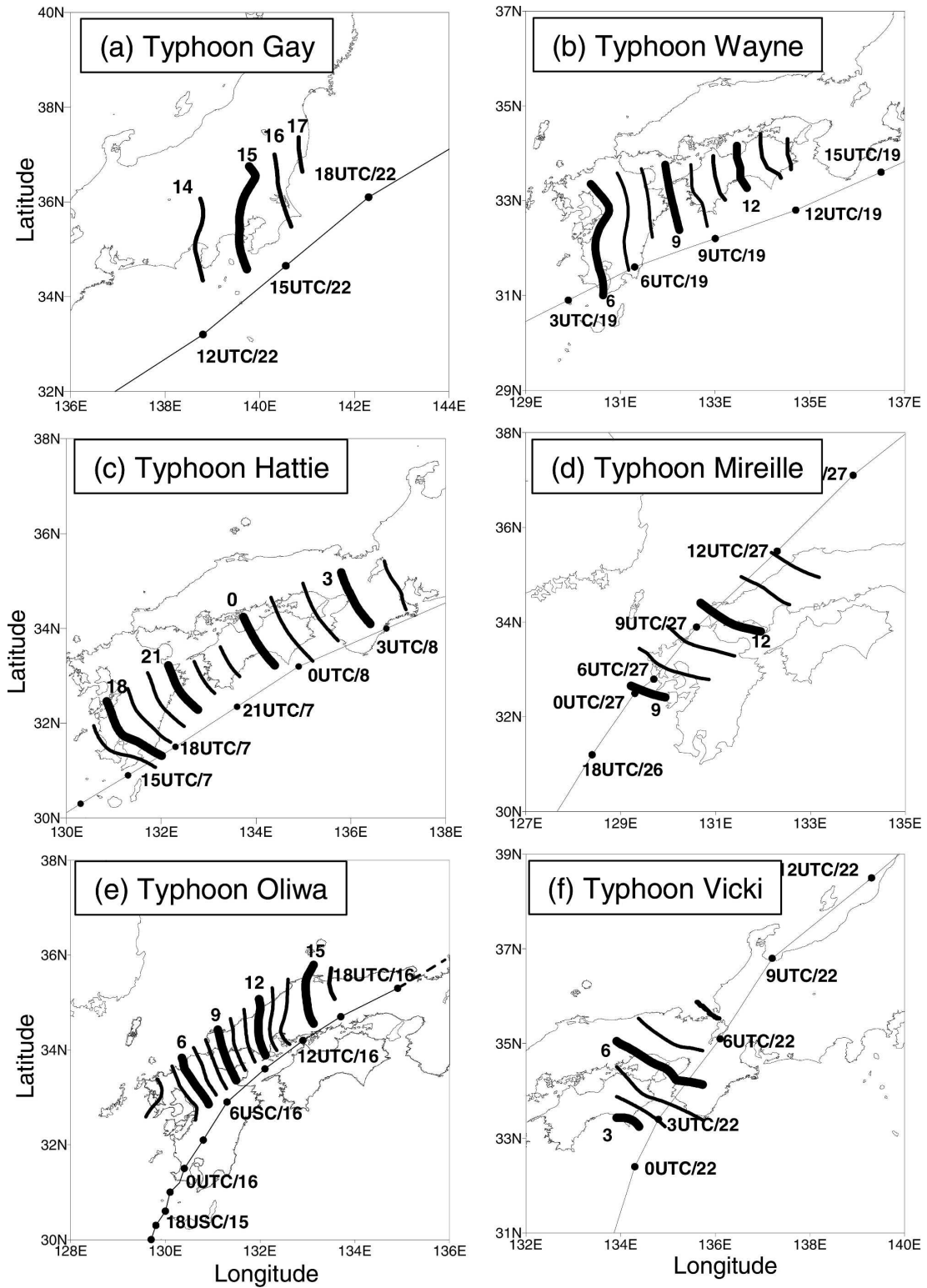
FIG. 16. Progressive locations of the pressure dip axis (solid lines) and accompanying typhoons (black circles) for Typhoons (a) Gay, (b) Wayne, (c) Hattie, (d) Mireille, (e) Oliwa, and (f) Vicki. Positions of typhoon centers, tracked at 3-h intervals, are denoted by closed circles. Hourly and 3-hourly locations of the pressure dip axis are indicated by thin and thick lines, respectively.
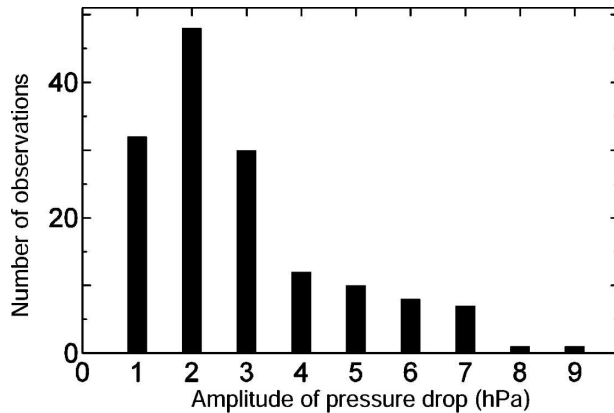
FIG. 17. Amplitude of the pressure drop recorded at different stations.

FIG. 18. Locations of the pressure dip axis relative to each typhoon center based on geographic coordinates.

from 7 to 9 October 1990 (Fig. 16c). The pressure dip axis extending from the southeast to the northwest occurred along the southern coast of the Japanese islands. Typhoon Mireille passed over the western coast of the Japanese islands in late September 1991 (Fig. 16d). On this occasion, the pressure dip axis extended from east-southeast to west-northwest and was observed in the northern part of Kyushu and the western part of the Chugoku district. Typhoon Oliwa made landfall on the southern part of Kyushu in mid-September 1997 (Fig. 16e). The pressure dip axis associated with Oliwa extended from south to north, appearing from southern Kyushu to the western Chugoku district. Typhoon Vicki traveled over the Kinki district in late September 1998 (Fig. 16f) and was accompanied by an east-southeast to west-northwest oriented pressure dip axis.

Figure 17 presents the amplitude of pressure dips recorded at various meteorological stations. The recorded amplitudes ranged from 1 to 9 hPa, with a typical value of 2 hPa, while the observed pressure dips were generally of 20–40-min duration (not shown). These values are similar to those reported in previous studies (e.g., Fujita 1992). There is no apparent relationship between the amplitude of the pressure dips and the speed and intensity of the associated typhoons (not shown).

Figure 18 shows the geographical locations of the pressure dip axes with respect to the centers of the typhoons. All the pressure dip axes were located to the west of the typhoon centers, with the majority within the northwestern quadrant. The distance between the pressure dip axes and the accompanying typhoon centers ranged from 50–300 km. All subsequent references to location relative to the typhoon center are described relative to the direction of movement of the typhoon. Fujita (1952) reported that pressure dips appeared on
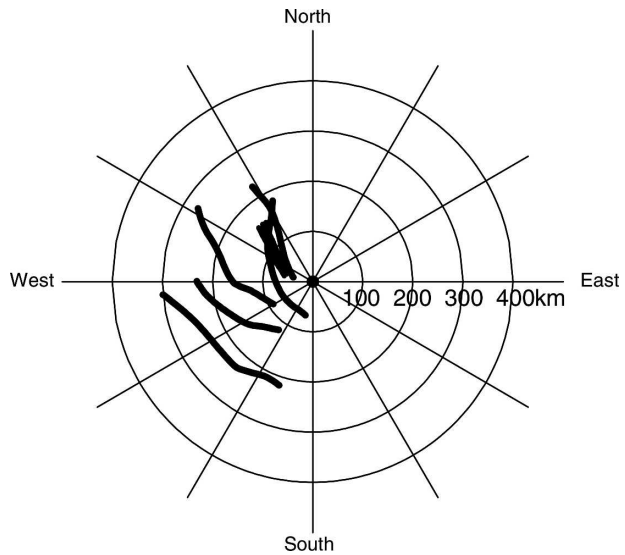
both the left- and right-hand sides of Typhoon Della, but that the pressure dip on the left-hand side of the typhoon had an amplitude of 7 hPa, while those on the right-hand side had a lesser amplitude. Nakajima et al. (1980) documented pressure dips on both the left- and right-hand sides of Typhoon Owen, but the dip on the right-hand side of the typhoon lasted only several hours and was weaker than the dip to the left of the typhoon. In all other documented cases, pressure dips were observed only to the left of the typhoon centers. Becasue all typhoons with pressure dips moved northeastward, we can also conclude that the occurrence of pressure dips with a significant amplitude and duration are confined to the left and the rear of the direction of the typhoon's movement.

Figure 19 shows the rainfall patterns when the dip associated with each typhoon has its maximum peak. As described earlier in the case of Typhoon Zeb (Fig. 6), there is a remarkable change in rainfall intensity across the pressure dip axis. The intense rainfall region occurs in advance of the pressure dip axis, while little rainfall is recorded following the passing of the pressure dip axis. Thus, the cessation of rainfall around pressure dips is a common feature of this phenomenon.

b. Simulation of pressure dips

To confirm the process of pressure dip formation described for Typhoon Zeb, we examined the structure of the simulated pressure dips associated with other typhoons. Figure 20 shows the simulated sea level pressure in D2 for five typhoons (Wayne, Hattie, Mireille,
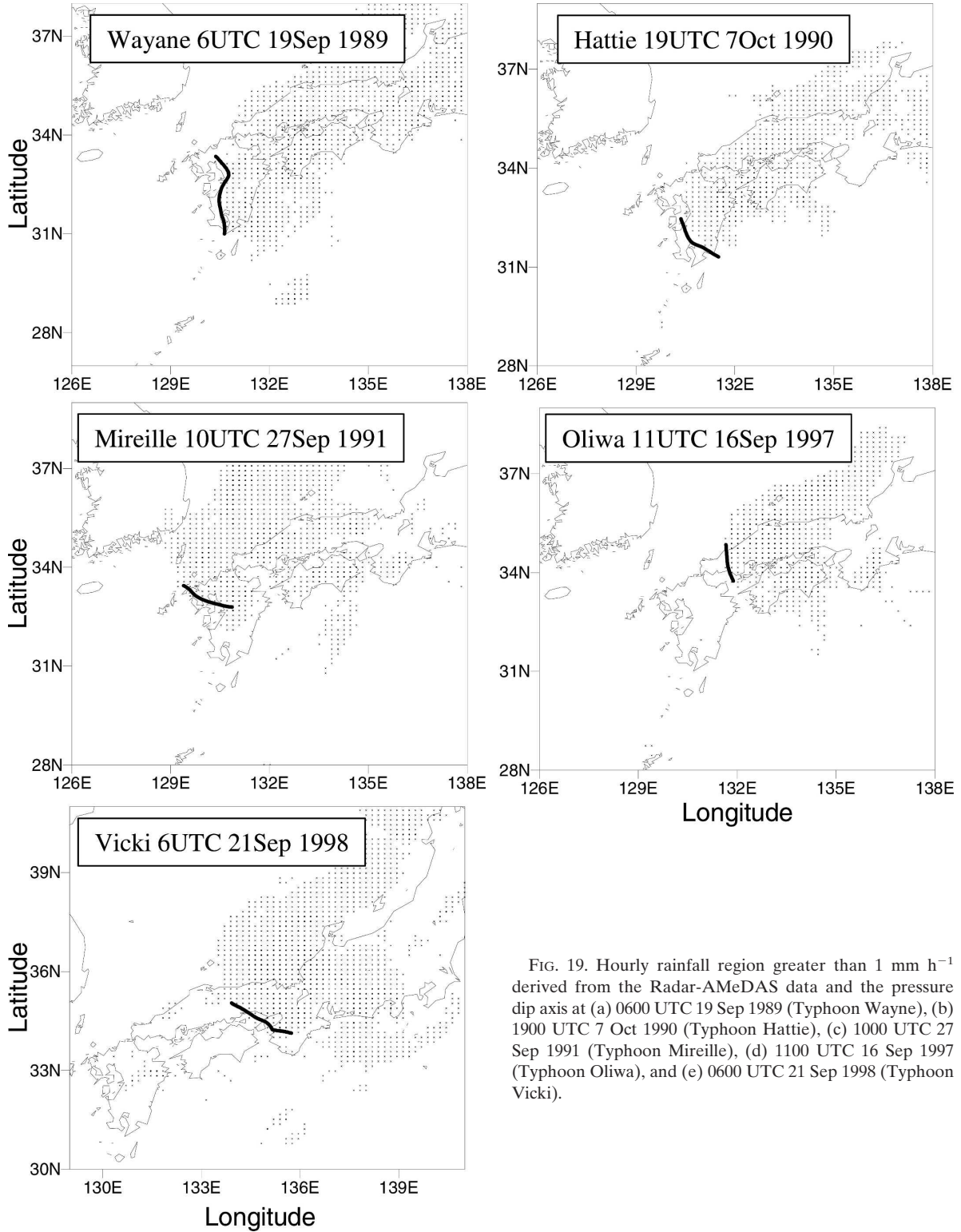
FIG. 19. Hourly rainfall region greater than 1 mm h^{-1} derived from the Radar-AMeDAS data and the pressure dip axis at (a) 0600 UTC 19 Sep 1989 (Typhoon Wayne), (b) 1900 UTC 7 Oct 1990 (Typhoon Hattie), (c) 1000 UTC 27 Sep 1991 (Typhoon Mireille), (d) 1100 UTC 16 Sep 1997 (Typhoon Oliwa), and (e) 0600 UTC 21 Sep 1998 (Typhoon Vicki).

Oliwa, and Vicki) at the time when the pressure dips were most developed. Warm potential temperature anomalies exist in the lower troposphere over the pressure dip axis (Fig. 21). Although the amplitudes of the simulated pressure dips are somewhat different from the observed values, the simulated pressure dip was closely related to deficiencies in the simulated warm potential temperature anomalies in the lower tropo-
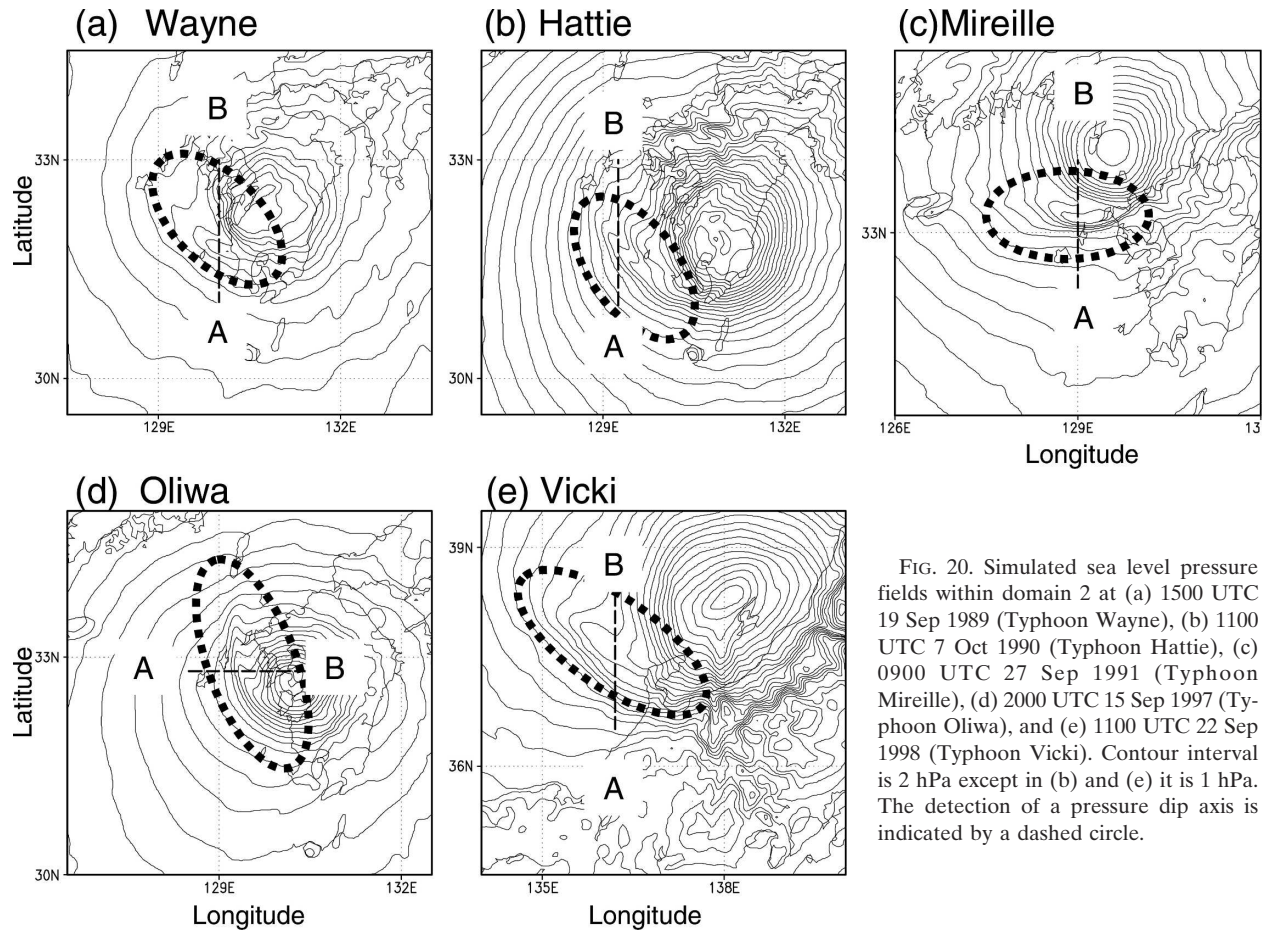
FIG. 20. Simulated sea level pressure fields within domain 2 at (a) 1500 UTC 19 Sep 1989 (Typhoon Wayne), (b) 1100 UTC 7 Oct 1990 (Typhoon Hattie), (c) 0900 UTC 27 Sep 1991 (Typhoon Mireille), (d) 2000 UTC 15 Sep 1997 (Typhoon Oliwa), and (e) 1100 UTC 22 Sep 1998 (Typhoon Vicki). Contour interval is 2 hPa except in (b) and (e) it is 1 hPa. The detection of a pressure dip axis is indicated by a dashed circle.

sphere. These results strongly support the conclusion that the pressure dips associated with the other typhoons have a comparable structure and formative process to that described in previous sections for the case of Typhoon Zeb. The pressure dips observed within Typhoon Gay, however, were not successfully simulated. The pressure dip recorded within Typhoon Gay may have been generated by a different mechanism, such as an internal gravity wave excited by the convection of the typhoon (Matsumoto and Okamura 1985). However, the exact reason for the inability to properly simulate the pressure in Typhoon Gay remains unclear.

6. Discussion

The present study suggests that the formation mechanism of a pressure dip is similar to that of a wake low (e.g., Johnson and Hamilton 1988; Johnson 2001). A wake low generally appears near or just behind the squall lines, in association with warming caused by unsaturated descent. The descending flow plays a role in the formation of the warming and is connected to rear inflow into the squall line (Johnson and Hamilton

1988). Past studies propose several hypotheses regarding the causes of the strong descending flow (Miller and Betts 1977; Johnson and Hamilton 1988; Zhang and Gao 1989; Schmidt and Cotton 1990; Gallus 1996). In addition, it is suggested that the environmental flow in which the squall line occurs determines the intensity of the rear inflow into the squall line at the middle and upper troposphere.

In the case of pressure dips, the midlatitude westerlies corresponding to rear inflows are extremely strong (see Fig. 23), while many wake lows have weaker rear inflow into the squall line at the middle and upper troposphere (Houze 1993). The midlevel confluence between the typhoon's circulation and the midlatitude westerlies is linked to the formation of a steep upward-sloping westward front at midlevels where an intense downdraft develops. A pressure dip therefore appears to be caused by the effect of the intense midlatitude westerlies on typhoons.

Previous studies (Uccellini and Koch 1987; Ramamurthy et al. 1993; Koch and Siedlarz 1999) have investigated the large pressure fluctuations associated
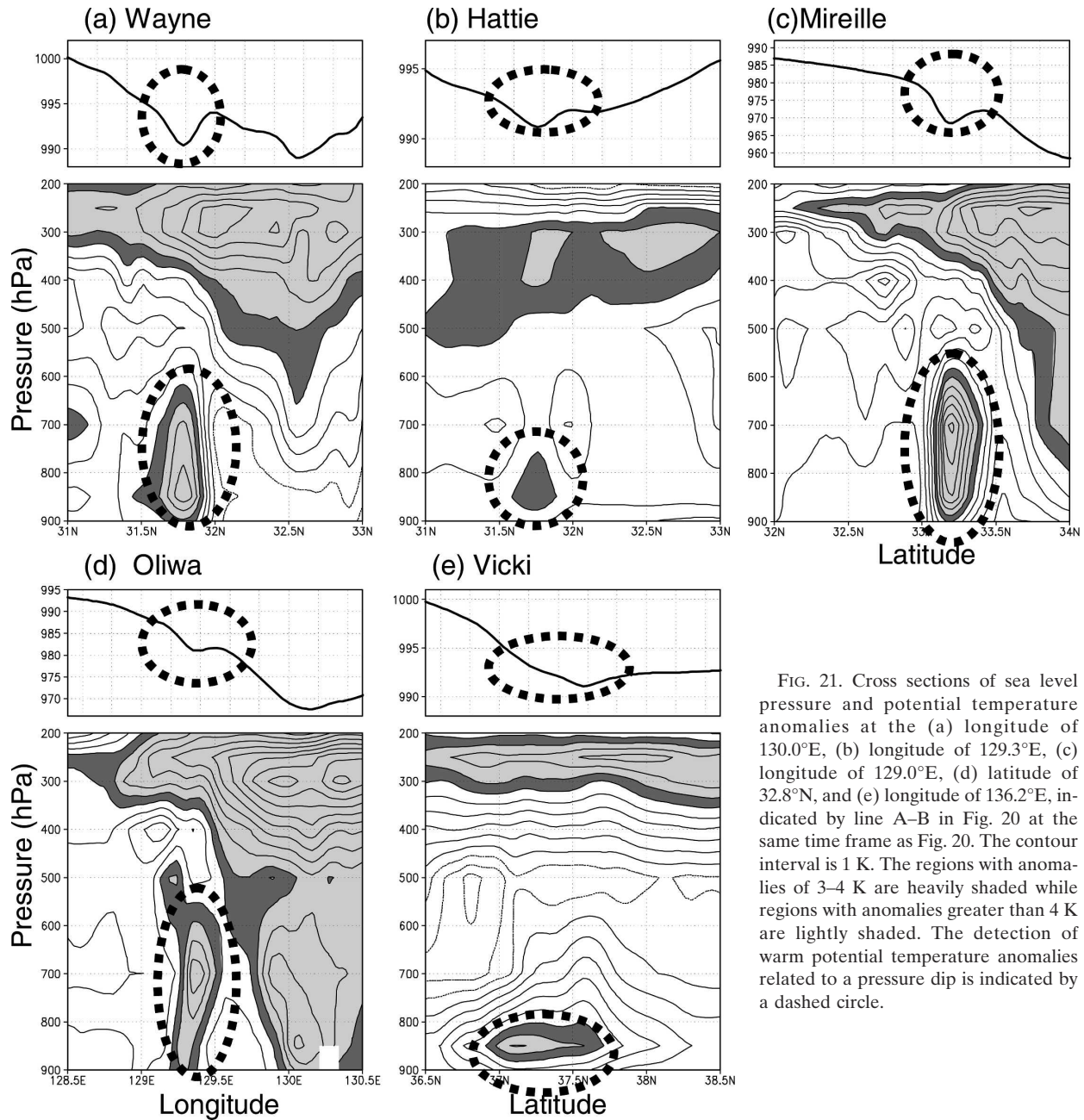
FIG. 21. Cross sections of sea level pressure and potential temperature anomalies at the (a) longitude of 130.0°E, (b) longitude of 129.3°E, (c) longitude of 129.0°E, (d) latitude of 32.8°N, and (e) longitude of 136.2°E, indicated by line A–B in Fig. 20 at the same time frame as Fig. 20. The contour interval is 1 K. The regions with anomalies of 3–4 K are heavily shaded while regions with anomalies greater than 4 K are lightly shaded. The detection of warm potential temperature anomalies related to a pressure dip is indicated by a dashed circle.

with extratropical cyclones, which are somewhat similar to the characteristics of pressure dips. They suggested that the fluctuations were excited by internal gravity waves through a geotropic adjustment process and shearing instability. Although the above process may be important for the generation of some pressure dips, for example, those recorded within Typhoon Gay (Matsumoto and Okamura 1985), the simulated results in the present study indicate that downdrafts play a fundamental role in the formation of pressure dips.

Ritchie and Elsberry (2001) used a mesoscale nu-

merical model to study the transition from tropical cyclones to extratropical cyclones. Under ideal baroclinic conditions, a tropical cyclone undergoing transformation develops a low-level warm anomaly to the west-southwest of the cyclone, which has similar characteristics to the pressure dip. The results of this study and of Ritchie and Elsberry's (2001) study demonstrate that a tropical cyclone undergoing transformation within midlatitude, large-scale, atmospheric conditions generates a diplike structure in surface pressure. Thus, one could conclude that a pressure dip is a unique phenomenon
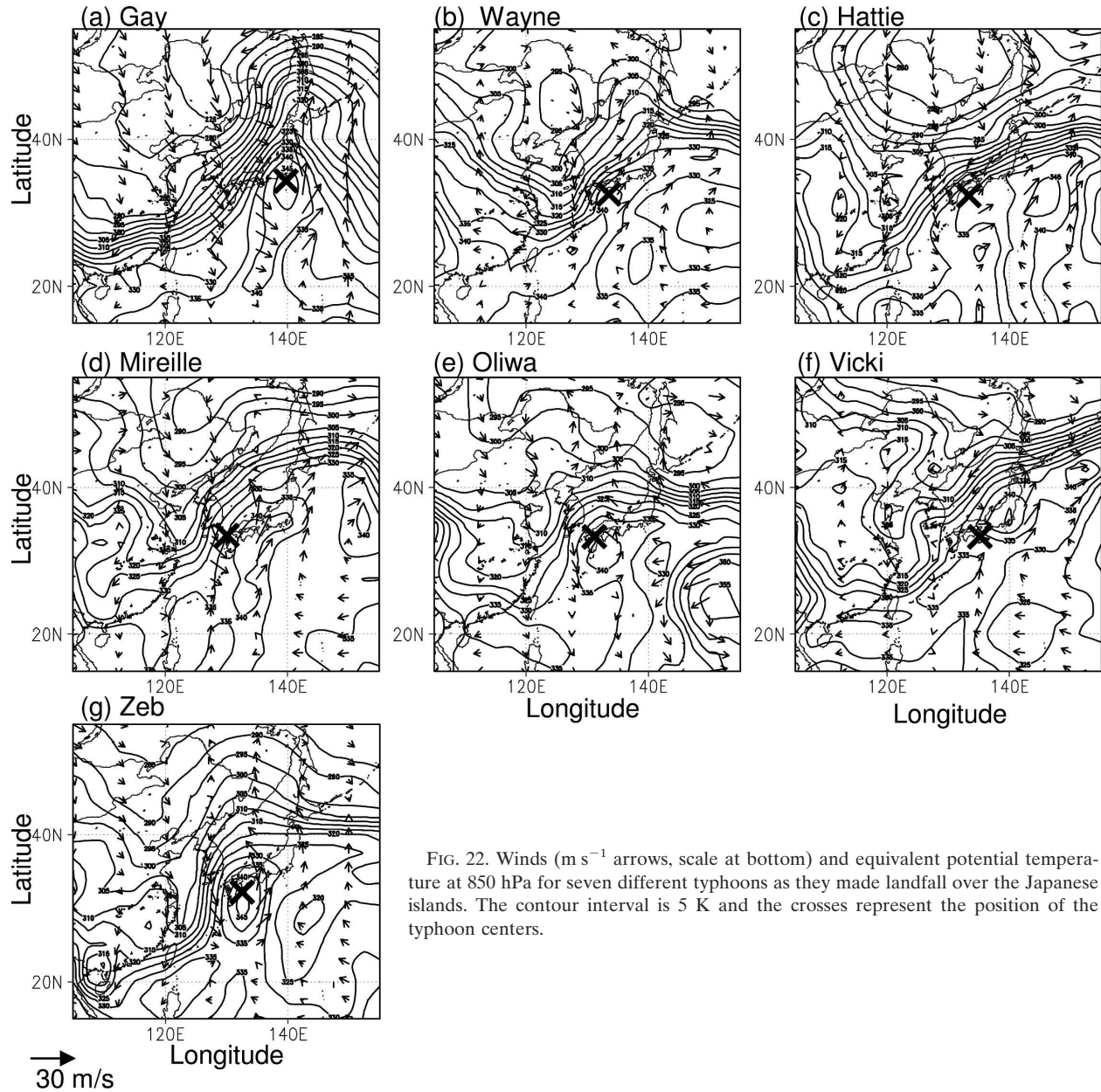
FIG. 22. Winds (m s^{-1} arrows, scale at bottom) and equivalent potential temperature at 850 hPa for seven different typhoons as they made landfall over the Japanese islands. The contour interval is 5 K and the crosses represent the position of the typhoon centers.

intrinsic to the transition of a tropical cyclone, although not every transforming typhoon is accompanied by the development of a pressure dip.

Figure 22 shows the potential temperature and wind at 850 hPa, while Fig. 23 shows the T_{BB} and wind at 500 hPa at the time when each of the typhoons listed in Table 2 made landfall in the Japanese islands. In all cases, there were steep thermal gradients in the low levels to the north and west of the typhoon centers. As mentioned in section 3, sudden changes in surface temperature and dewpoint temperature that preceded the arrival of the pressure dips (Fig. 1) are related to the influence of the surface fronts. At the mid- and upper troposphere, there is a cloudy region known as the delta rain shield (Shimazu 1998), which extends northeast from the typhoon centers (Fig. 23). The midlatitude westerlies are present in the Japanese islands, accompanied by a trough to the west of Japan. Such large-scale atmospheric flow is favorable for the northeast movement of typhoons across the Japanese islands and for the detection of pressure dips at land-based meteorological stations. These features are the characteristics of a typhoon moving into the midlatitude areas of strong baroclinicity.
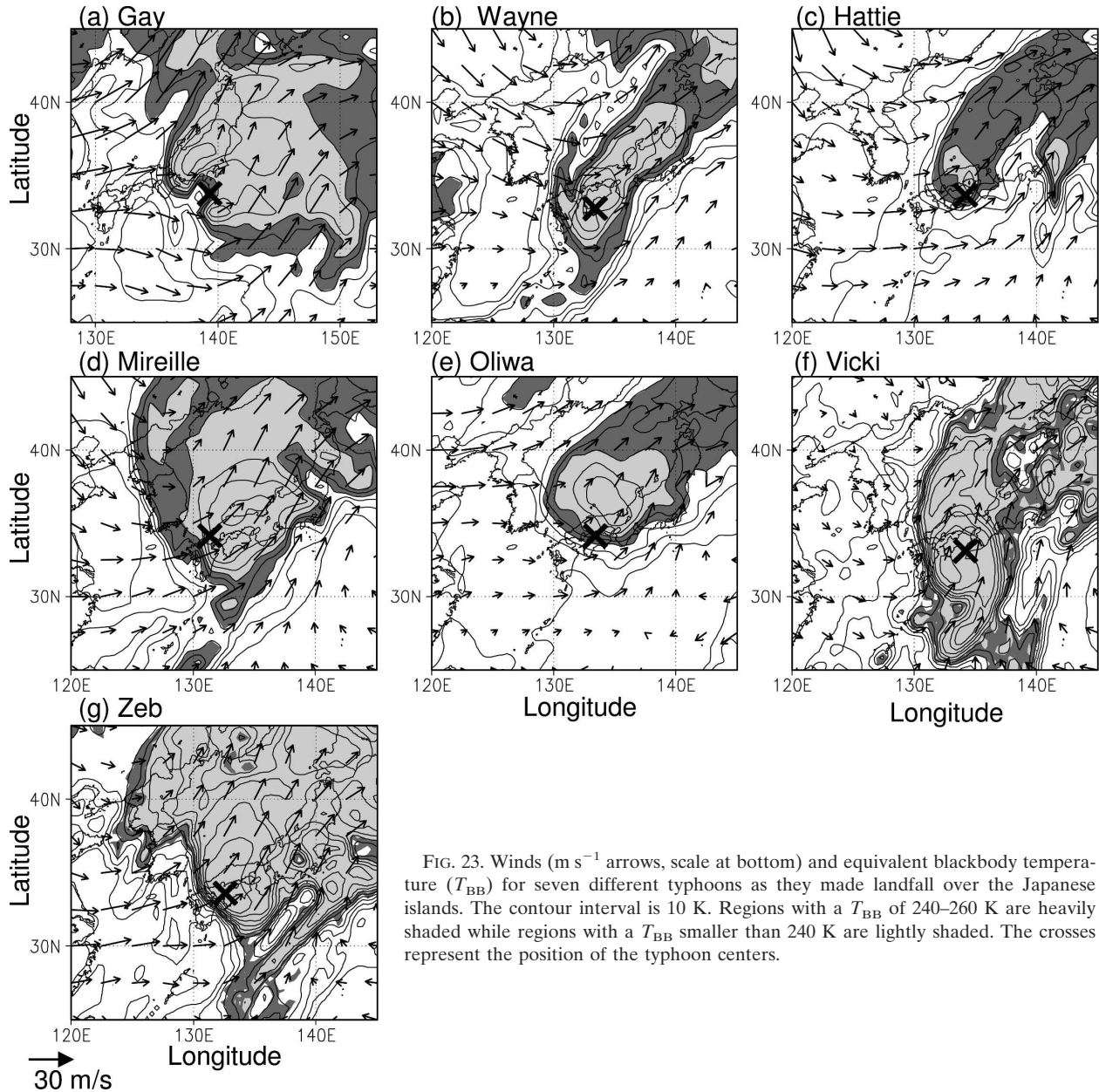
FIG. 23. Winds (m s^{-1} arrows, scale at bottom) and equivalent blackbody temperature (T_{BB}) for seven different typhoons as they made landfall over the Japanese islands. The contour interval is 10 K. Regions with a T_{BB} of 240–260 K are heavily shaded while regions with a T_{BB} smaller than 240 K are lightly shaded. The crosses represent the position of the typhoon centers.

It is interesting to note that the pressure dips were only observed during September and October (Table 2), when the atmospheric conditions described above develop most commonly. Pressure dips reported in previous studies were also associated with typhoons that crossed Japan during September and October (e.g., Nakajima et al. 1980). One notable exception is Typhoon Della, which made landfall in June 1949 (Fujita 1952). Although the conditions described above also occur during June and early July, typhoons rarely make landfall over Japan. Typhoons most frequently cross Japan in late July and August, but pressure dips are not observed during the summer because the westerly winds retreat to the north. Thus, it would appear that pressure dips tend to occur in September and October when a typhoon enters the zone of midlatitude westerlies. The atmospheric conditions described above might be favorable for the transformation of the typhoon structure into an extratropical storm (Muramatsu 1982; Kitabatake 2002). The typhoons that had pressure dips were of considerable intensity at the time they approached the Japanese islands. These typhoons then rapidly weakened and eventually transformed into extratropical cyclones during their passage over the Japanese islands.

The area of downdraft overlapped with the confluence zone generated by the interaction between the typhoon's circulation and the environmental westerly winds as the typhoon entered the zone of midlatitude westerlies (Fig. 11). Although the same formation mechanism was found to the north and south of the typhoon center in our simulations, pressure dips were discernible only over that part of the downdraft region on the western side of the typhoon center (Figs. 8 and 18). The intensity of confluence between the typhoon's circulation and the environmental westerly winds affected the relative amount of dry air entering the moist region at mid- and upper level, which in turn contributed to the difference in the intensity of the downdraft. The downdraft to the north was not intense enough to form the pressure dip (Fig. 11). On the other hand, the amplitude of the pressure dips was related to the potential temperature anomalies, which were the deviations from environmental potential temperature. The environmental low-level potential temperature to the south, the warm region of the surface front (Fig. 22), was relatively warm. Therefore, warm potential temperature anomalies related to a pressure dip in lower levels tended to develop only on the western side of the typhoon center and to the north of the surface front where there was advection of cold air (see Fig. 24). This explains why pressure dips appeared only in limited areas although the downdrafts occurred over a relatively elongated area. Furthermore, the northeastward movement of the typhoon and the locational difference between the midlevel and surface fronts (see Fig. 24a) caused the frontal passage prior to the pressure dip to be unobserved at stations far from the track of the typhoon, as described in section 3a.

After analyzing U.S. hurricanes and Japanese typhoons, Fujita (1992) noted that there are two different types of pressure dips: (i) cold-sector dips, which form in the wake of a rainband in the northwestern sector, and (ii) warm-sector dips, which form in any sector of the storm where there is free cold-air inflow. The former type is similar to the pressure dips considered here while the latter type seems to correspond to pressure dips that we excluded in the present study. However, because of the limitations of the available data, the characteristics of the pressure dips associated with hurricanes are not clear. Such an examination could be considered for future study.

7. Summary

We simulated the pressure dips associated with Typhoon Zeb using a mesoscale numerical model. The model successfully reproduced the major features of
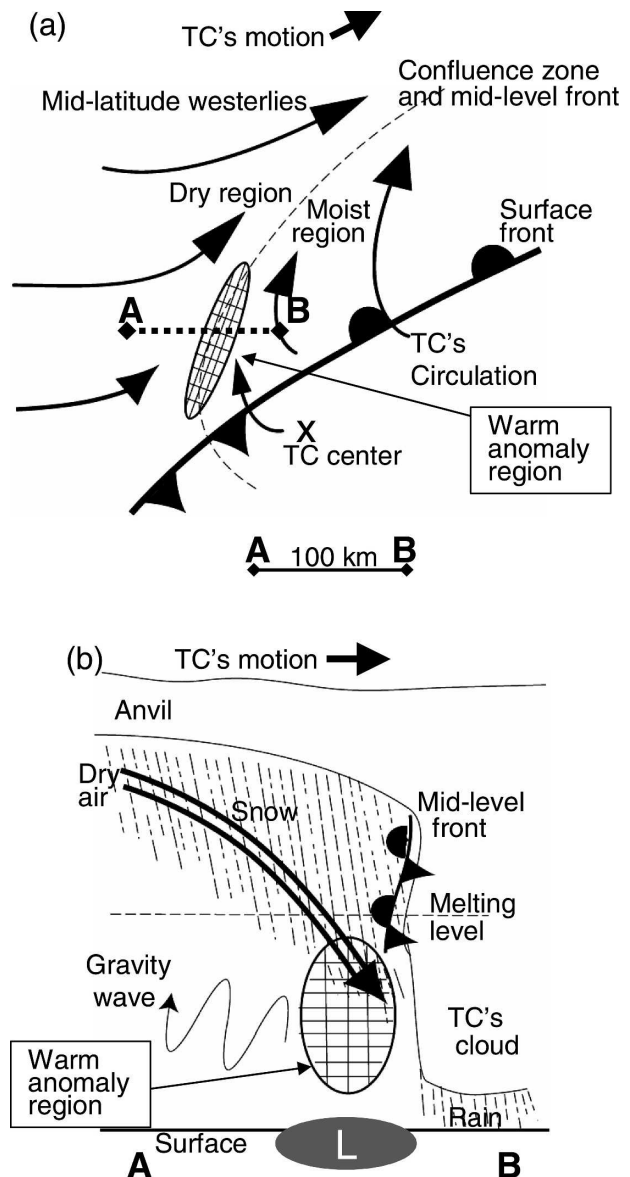

FIG. 24. Schematic of the (a) circulation around the pressure dip and (b) cross section through the pressure dip indicated by the line A–B in (a). Arrows in (a) indicate streamlines at the midlevel while those in (b) indicate the trajectories of the upper dry air. The broken line in (a) is the confluence zone and equivalent potential temperature fronts resulting from the interaction between the typhoon's circulation and the environmental westerly winds at the midlevel. The frontal symbols indicate fronts, the broken line in (b) is the melting level, and the letter L refers the surface low pressure region (i.e., pressure dip). The cross represents the position of the typhoon center. The hatched regions indicate the region of warm potential temperature anomaly related to the pressure dip. Note that horizontal scales differ in the two schematics.

pressure dips and thus permitted us to investigate the formation mechanism of the pressure dips.

The formation mechanism of the pressure dips is illustrated schematically in Fig. 24. The simulated pressure dips were closely linked to warm potential temperature anomalies in the lower troposphere, which are accompanied by downdrafts throughout the entire troposphere. In association with the anomalies, relative humidity and rainwater decreased while an overhanging anvil above the melting level developed. As the typhoon moved into the midlatitude westerlies, the confluence zone and equivalent potential temperature fronts resulting from the interaction between the typhoon's circulation and the environmental westerly winds appeared at midlevel and the inflow of a dry air mass occurred (Fig. 24a). As dry air carried by the midlatitude westerlies entered the moist region below the anvil, the cooling of evaporation and sublimation caused negative buoyancy, which resulted in the formation of downdrafts (Fig. 24b). The parcels underwent accelerated evaporation until passing the melting level. Below the melting levels, where there were fewer hydrometeors, evaporative cooling was insufficient to offset adiabatic warming. As a result, the warm potential temperature anomalies occurred in the lower levels, resulting in the formation of pressure dips. The warm potential temperature anomalies related to a pressure dip in lower levels tended to develop only on the western side of the typhoon center and to the north of the surface front. The horizontal scale of pressure dips was determined by the width of the region of mesoscale downdrafts around the melting level. Similar processes were found to operate during the simulation of pressure dips associated with other typhoons.

In the present study, we have also described the features of pressure dips observed during the period from 1980 to 1998 using barographic data from different meteorological stations. During this period, pressure dips of significant amplitude and duration were recorded in 7 out of 89 typhoons with at least tropical cyclone intensity. The observed pressure dips occurred only on the western side of the typhoon centers, at a distance of 50–300 km from the typhoon center, and were accompanied by a sudden cessation of rainfall. All of these typhoons moved rapidly toward the northeast or north-northeast during their passage over the Japanese islands before weakening rapidly and eventually transforming into extratropical cyclones. The pressure dips were observed under large-scale environmental conditions characterized by westerly winds associated with a midlatitude trough with a dry air mass to the west of Japan at upper levels and fronts at lower levels. The pressure dips were detected in typhoons that occurred during the boreal autumn when the above large-scale environmental conditions appear around Japan. No pressure dips were observed in typhoons during the Northern Hemisphere's summer when most typhoons approach Japan. We therefore would suggest that a pressure dip is an inherent feature of the asymmetric structure of a typhoon undergoing extratropical transition.

The proportion of typhoons associated with pressure dips may be higher than the detected numbers because we were only able to detect pressure dips in typhoons that passed directly over the Japanese islands. It may be possible to find more pressure dips in typhoons that are located solely over the Pacific Ocean from high-resolution satellite data. Such data would increase our ability to understand the characteristics of meso-β-scale atmospheric phenomena associated with tropical cyclones, including pressure dips, and lead to a better understanding of tropical cyclones.

REFERENCES

Anthes, R. A., E.-Y. Hsie, and Y.-H. Kuo, 1987: Description of the Penn State/NCAR Mesoscale Model Version 4 (MM4). NCAR Tech. Note NCAR/TN-282+STR, 66 pp. [Available from NCAR Publications Office, P.O. Box 3000, Boulder, CO 80307-3000.]

Dudhia, J., 1989: Numerical study of convection observed during the winter monsoon experiment using a mesoscale two-dimensional model. *J. Atmos. Sci.,* **46,** 3077–3107.

——, 1993: A nonhydrostatic version of the Penn State–NCAR Mesoscale Model: Validation tests and simulation of an Atlantic cyclone and cold front. *Mon. Wea. Rev.,* **121,** 1493–1513.

Fudeyasu, H., and O. Tsukamoto, 2000: Pressure dip observed in the Typhoon 9810 (in Japanese). *Tenki,* **47,** 443–451.

Fujii, T., 1992: Meteorological characteristics of high wind of Typhoon 9119 (Mireille) (in Japanese). *J. Wind Eng.,* **53,** 27–35.

Fujita, T., 1952: Study on pressure dips within Typhoon Della. *Bull. Kyushu Inst. Technol. Sci. Technol.,* **2,** 52–61.

——, 1992: *Japanese Typhoons, Mystery of Severe Storms*. University of Chicago, 298 pp.

Gallus, W. A., Jr., 1996: The influence of microphysics in the formation of intense wake lows: A numerical modeling study. *Mon. Wea. Rev.,* **124,** 2267–2281.

Grell, G. A., 1993: Prognostic evaluation of assumptions used by cumulus parameterizations. *Mon. Wea. Rev.,* **121,** 764–787.

——, J. Dudhia, and D. R. Stauffer, 1995: A description of the fifth-generation Penn State/NCAR Mesoscale Model (MM5). NCAR Tech. Note NCAR/TN–398+STR, 138 pp. [Available from NCAR Publications Office, P.O. Box 3000, Boulder, CO 80307-3000.]

Hong, S.-Y., and H.-L. Pan, 1996: Nonlocal boundary layer vertical diffusion in a medium-range forecast model. *Mon. Wea. Rev.,* **124,** 2322–2339.

Houze, R. A., Jr., 1993: *Cloud Dynamics.* Academic Press, 573 pp.

Inoue, T., K. Yoshida, A. Tabata, H. Tanaka, and K. Sakamoto, 1999: A sharp pressure dip observed in the Typhoon T9810 (Zeb) (in Japanese). *Bull. Kobe Mar. Obs.,* **218,** 1–10.

Johnson, R. H., 2001: Surface mesohighs and mesolows. *Bull. Amer. Meteor. Soc.,* **82,** 13–31.

——, and P. J. Hamilton, 1988: The relationship of surface pressure features to the precipitation and airflow structure of an intense midlatitude squall line. *Mon. Wea. Rev.,* **116,** 1444–1472.

Kalnay, E., and Coauthors, 1996: The NCEP/NCAR 40-Year Reanalysis Project. *Bull. Amer. Meteor. Soc.,* **77,** 437–471.

Kitabatake, N., 2002: Extratropical transformation of Typhoon Vicki (9807): Structural change and the role of upper-tropospheric disturbances. *J. Meteor. Soc. Japan,* **80,** 229–247.

Koch, S. E., and C. O'Handley, 1997: Operational forecasting and detection of mesoscale gravity waves. *Wea. Forecasting,* **12,** 253–281.

——, and L. M. Siedlarz, 1999: Mesoscale gravity waves and their environment in the central United States during STORM-FEST. *Mon. Wea. Rev.,* **127,** 2854–2879.

Maeda, H., 1994: On the pressure dip within Typhoon 9119 (in Japanese). *J. Meteor. Res. Japan,* **46,** 25–38.

Matsumoto, S., and H. Okamura, 1985: The internal gravity wave observed in the Typhoon T8124 (Gay). *J. Meteor. Soc. Japan,* **63,** 37–51.

Muramatsu, T., 1982: Extratropical transformation of mature typhoon: The case study of Typhoon 7916, Owen (in Japanese). *Tenki,* **29,** 1199–1212.

Miller, M. J., and A. K. Betts, 1977: Traveling convective storms over Venezuela. *Mon. Wea. Rev.,* **105,** 833–848.

Nakajima, C., Y. Mitsuta, Y. Gocho, M. Tanaka, T. Fujii, and N. Monji, 1980: On Typhoon 7916 (in Japanese). *Disaster Prev. Res. Inst. Kyoto Univ. Bull.,* **23,** 87–111.

Obayashi, M., 1991: Data processing in the system for very short-range forecast of precipitation (in Japanese). *Sokko-Jihou,* **58,** 189–207.

Ramamurthy, M. K., R. M. Rauber, B. P. Collins, and N. K. Malhotra, 1993: A comparative study of large-amplitude gravity wave events. *Mon. Wea. Rev.,* **121,** 2951–2974.

Ritchie, E. A., and R. L. Elsberry, 2001: Simulations of the transformation stage of the extratropical transition of tropical cyclones. *Mon. Wea. Rev.,* **129,** 1426–1480.

Schmidt, J. M., and W. R. Cotton, 1990: Interactions between upper and lower troposphere gravity waves on squall line structure and maintenance. *J. Atmos. Sci.,* **47,** 1205–1222.

Shimazu, Y., 1998: Classification of precipitation systems in mature and early weakening stage of typhoon around Japan. *J. Meteor. Soc. Japan,* **76,** 437–445.

Tsujimura, Y., 1993: Meteorology, soliton and modon (in Japanese). *Meteor. Res. Note,* **178,** 73–79.

Uccellini, L. W., and S. E. Koch, 1987: The synoptic setting and possible energy sources for mesoscale wave disturbances. *Mon. Wea. Rev.,* **115,** 721–729.

Zhang, D.-L., and K. Gao, 1989: Numerical simulations of an intense squall line during 10–11 June 1985 PRE-STORM. Part II: Rear inflow, surface pressure perturbations, and stratiform precipitation. *Mon. Wea. Rev.,* **117,** 2067–2094.